Table of Contents

1. Synthesis

1.1. Materials and Methods

Starting materials 1,3,5-tris(4-bromophenyl)benzene, 4-formylphenylboronic acid, 1,3,5-tris(bromomethyl)benzene, phenylacetonitrile, and $Pd(OAc)_2$, as well as reagents and solvents, were purchased from TCI, Sigma-Aldrich, PMO Pty Ltd, Fluka, or Penta, and were used as obtained without further purification. The solvents were evaporated on a Heidolph Laborota 4001. The Suzuki-Miyaura cross-coupling reaction was carried out in a Schlenk flask under an inert atmosphere of argon. The solvothermal Knoevenagel reactions were performed in 2 mm thick-walled glass tubes under vacuum (1–2 Torr). The column chromatography was performed on silica gel (SiO_2 60, particle size 0.040–0.063 mm, Merck) using commercially available solvents. Thin-layer chromatography was performed on aluminum plates coated with SiO_2 60 F254 silica gel (Merck) and visualized under UV lamp (254 or 365 nm). Melting points were determined in open capillaries on a Büchi B-540 instrument. The mass spectra were measured on a GC/EI-MS configuration consisting of an Agilent 7890B Series GC Custom gas chromatograph. Elemental analysis was performed on a Flash 2000 CHNS Elemental Analyzer.

1.2. Synthesis of 1,3,5-Tris(4-formylbiphenyl)benzene (TFBB)

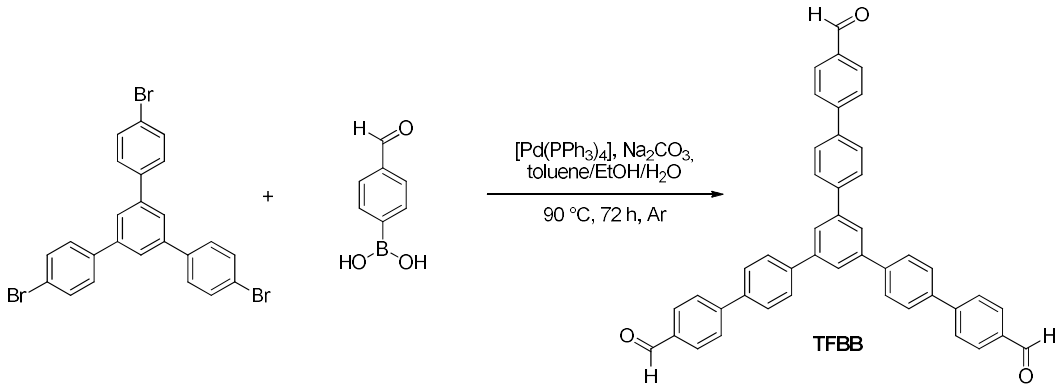

The reaction was carried out according to a slightly modified literature procedure.[1] 1,3,5-Tris(4-bromophenyl)benzene (1 g, 1.84 mmol) and 4-formylphenylboronic acid (993 mg, 6.62 mmol) were dissolved in a mixture of toluene (40 mL), EtOH (12 mL), and H_2O (8 mL), argon was bubbled through the solution for

[1] S. K. Das, S. Mishra, K. Manna, U. Kayal, S. Mahapatra, K. D. Saha, S. Dalapati, G. P. Das, A. A. Mostafa and A. Bhaumik, A new triazine based π-conjugated mesoporous 2D covalent organic framework: its *in vitro* anticancer activities, *Chem. Commun.*, 2018, **54**, 11475–11478.

10 min, whereupon [Pd(PPh$_3$)$_4$] (127 mg, 0.11 mmol) and Na_2CO_3 (878 mg, 8.28 mmol) were added, and the reaction was stirred under argon at 90 °C for 72 h. The solvents were evaporated under reduced pressure, and the resulting material was dissolved in DCM (100 mL). Saturated aqueous NH_4Cl (100 mL) was added, the organic phase was separated, the aqueous one was extracted with DCM (2×50 mL), the combined organic extracts were dried (Na_2SO_4), and the solvent was evaporated under reduced pressure. The crude product was purified by column chromatography (SiO_2; DCM/EtOAc 49:1). Yield: 838 mg (74 %). White solid. M. p. = 151–154 °C (lit.[2] 174–176 °C). R_f = 0.7 (SiO_2; DCM/EtOAc 49:1). ^{1}H NMR (500 MHz, 25 °C, $CDCl_3$): δ = 10.07 (s, 3H, CHO), 7.99–7.97 (m, 6H, Ar), 7.89 (s, 3H, Ar), 7.85–7.81 (m, 12H, Ar), 7.78–7.77 (m, 6H, Ar) ppm. ^{13}C NMR (125 MHz, 25 °C, $CDCl_3$): δ = 192.09, 146.70, 142.04, 141.23, 139.27, 135.55, 130.59, 128.18, 128.14, 127.80, 125.52 ppm. IR (neat): ν = 3030, 2818, 2728, 1699, 1602, 1388, 1214, 1167, 1003, 801, 498 cm^{-1}. HR-FT-MALDI-MS (DCTB) *m/z*: calculated for $C_{45}H_{30}O_3^+$ ([M]$^+$) 618.21895, found 618.21861 Da.

1.3. Synthesis of (Benzene-1,3,5-triyl)triacetonitrile (BTAN)

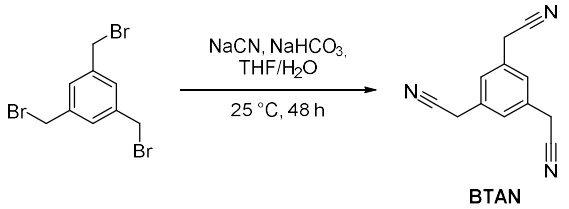

BTAN

The compound was synthesized according to a literature procedure.[3] 1,3,5-Tris(bromomethyl)benzene (2 g, 5.60 mmol) was dissolved in THF (20 mL), and $NaHCO_3$ (20 mL, sat. aq. sol.), NaCN (2.74 g, 56 mmol), and H_2O (20 mL) were gradually added. The reaction mixture was stirred at 25 °C for 48 h, carefully neutralized with 1M HCl, the precipitate was filtered off, washed with water several times, and dried *in vacuo* at 90 °C. Yield: 0.83 g (76 %). Yellowish solid. M. p. = 126–128 °C (lit.[4] 123–125 °C). ^{1}H NMR (500 MHz, 25 °C, $CDCl_3$): δ = 7.28 (s,

[2] S. Kotha, D. Kashinath, K. Lahiri and R. B. Sunoj, Synthesis of *C*$_3$-Symmetric Nano-Sized Polyaromatic Compounds by Trimerization and Suzuki–Miyaura Cross-Coupling Reactions, *Eur. J. Org. Chem.*, 2004, 4003–4013.

[3] E. Özdemir, D. Thirion and C. T. Yavuz, Covalent organic polymer framework with C–C bonds as a fluorescent probe for selective iron detection, *RSC Adv.*, 2015, **5**, 69010–69015.

[4] M. Kanishi, J.-I. Kunizaki, J. Inanaga and M. Yamaguchi, Synthesis of Macrocyclic [*n.n.n*](1,3,5)Cyclophane Polylactones, *Bull. Chem. Soc. Jpn.*, 1981, **54**, 3828–3831.

3H, Ar), 3.77 (s, 6H, CH_2) ppm. ^{13}C NMR (125 MHz, 25 °C, $CDCl_3$): δ = 132.53, 127.56, 117.16, 23.54 ppm. IR (neat): ν = 2945, 2917, 2248, 1609, 1465, 1411, 940, 828, 685, 439 cm^{-1}. EI-MS (70 eV) *m/z* (rel. in.): 195 ($[M]^+$, 30), 168 (17), 155 (100), 140 (7), 128 (14).

1.4. Synthesis of Model Compound (MC)

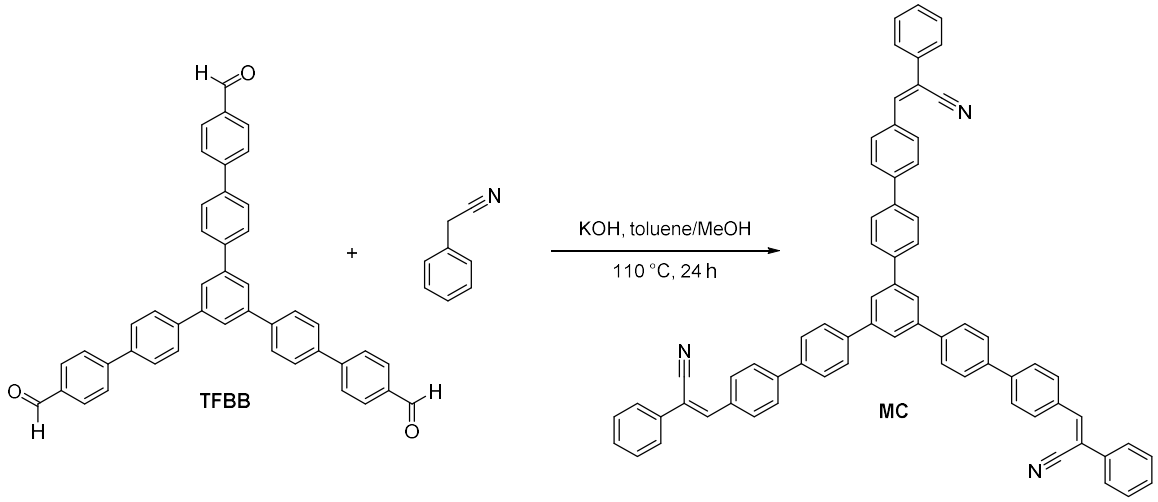

To the suspension of **TFBB** (200 mg, 0.32 mmol) and phenylacetonitrile (225 mg, 1.92 mmol) in toluene (40 mL), a solution of KOH (108 mg, 1.92 mmol) in MeOH (10 mL) was added. The reaction mixture was stirred at 110 °C for 24 h, cooled to 25 °C, and placed in an ice bath. The precipitate was filtered off and washed with MeOH (3×20 mL). The crude product was recrystallized from toluene. Yield: 124 mg (42 %). Yellow solid. ^1H NMR (500 MHz, 25 °C, DMSO-d_6): δ = 8.07–8.05 (m, 9H, Ar), 8.01–8.00 (m, 9H, Ar), 7.94–7.89 (m, 12H, Ar), 7.79–7.77 (m, 6H, Ar + CH=C), 7.54–7.51 (m, 6H, Ar), 7.46–7.43 (m, 3H, Ar) ppm. ^{13}C NMR (125 MHz, 25 °C, DMSO-d_6): δ = 142.33, 141.45, 141.06, 139.73, 138.22, 133.84, 132.89, 129.94, 129.32, 129.26, 127.90, 127.31, 127.02, 125.81, 124.42, 118.09, 109.90 ppm. IR (neat): ν = 3028, 2211, 1593, 1496, 1000, 900, 814, 759, 691, 520 cm^{-1}. HR-FT-MALDI-MS (DCTB) *m/z*: calculated for $C_{69}H_{45}N_3^+$ ($[M]^+$) 915.36080, found 915.36005 Da.

1.5. Synthesis of CN-COF

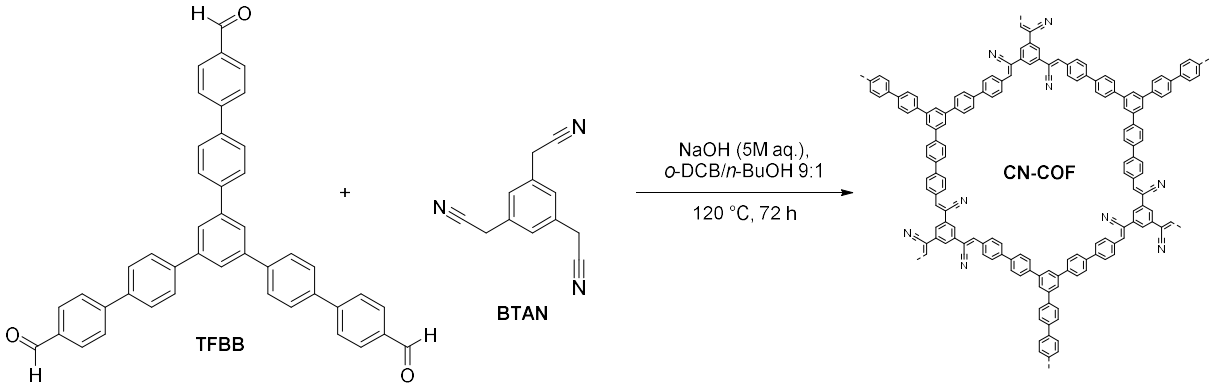

A glass tube was charged with **BTAN** (20 mg, 0.102 mmol) and **TFBB** (63 mg, 0.102 mmol), followed by *o*-DCB (2.7 mL), *n*-BuOH (0.3 mL), and NaOH (0.1 mL, 5M aq.). The reaction mixture was sonicated for 2 min, degassed through three freeze-pump-thaw cycles, sealed under vacuum, allowed to warm to laboratory temperature, and heated at 120 °C in an oil bath without disturbance for 72 h. After cooling to 25 °C, the solid was filtered off and washed with MeOH (3×10 mL), water (3×10 mL), and acetone (3×10 mL). The resulting COF was further Soxhlet-extracted using MeOH (24 h) and THF (24 h) and dried *in vacuo* at 110 °C for 8 h. Yield: 70 mg (90 %). Yellow fluffy powder. IR (neat): ν = 3029, 2213, 1697, 1595, 1496, 1003, 814, 514 cm^{-1}. Elemental analysis: calculated for $C_{57}H_{33}N_3$ (759.89) C 90.09, H 4.38, N 5.53, found C 85.32, H 4.47, N 4.42.

Table S1. Experiments carried out towards the synthesis of **CN-COF**.

Experiment	Solvent system	Base	Temperature time	Heating	Yield	Crystallinity
1	*o*-DCB	DBU (0.2 mL, 5M aq.)	120 °C, 72 h	oil bath	99 %	moderate
2	*o*-DCB	Cs_2CO_3 (3 equiv.)	120 °C, 72 h	oil bath	45 %	N/A
3	*o*-DCB/*n*-BuOH 9:1	Cs_2CO_3 (3 equiv.)	120 °C, 72 h	oil bath	32 %	low
4a[a]	*o*-DCB/*n*-BuOH 7:3	Cs_2CO_3 (3 equiv.)	120 °C, 72 h	oil bath	87 %	high
4b	*o*-DCB/*n*-BuOH 7:3	Cs_2CO_3 (3 equiv.)	120 °C, 72 h	drying oven	18 %	N/A
5a	*o*-DCB/*n*-BuOH 9:1	NaOH (0.2 mL, 5M aq.)	120 °C, 72 h	oil bath	92 %	moderate
5b	*o*-DCB/*n*-BuOH 9:1	NaOH (0.2 mL, 5M aq.)	120 °C, 72 h	drying oven	68 %	high
5c	*o*-DCB/*n*-BuOH 9:1	NaOH (0.1 mL, 5M aq.)	120 °C, 72 h	oil bath	90 %	high
6	*o*-DCB/*n*-BuOH 9:1	KOH (0.2 mL, 5M aq.)	120 °C, 72 h	oil bath	65 %	amorph

[a]Non-reproducible.

1.6. Synthesis of Pd@CN-COF

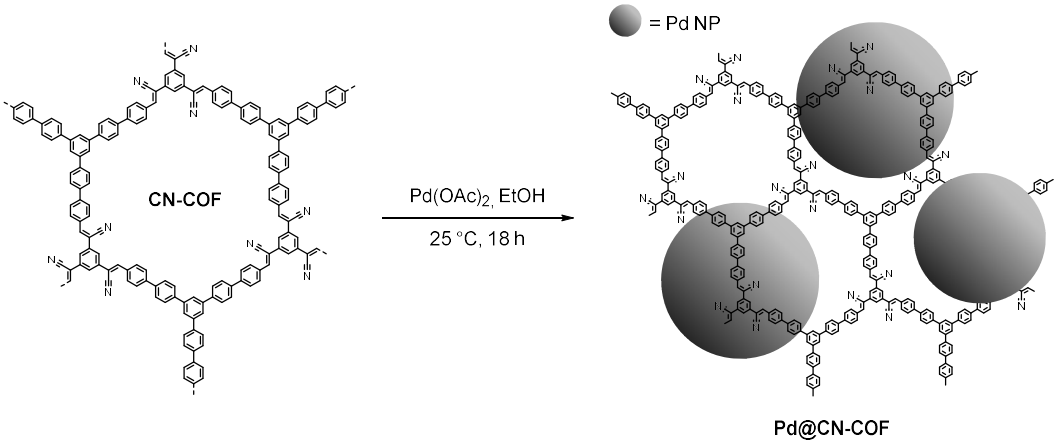

A suspension of **CN-COF** (50 mg, 0,066 mmol) and $Pd(OAc)_2$ (7.4 mg, 0.033 mmol) in absolute EtOH (30 mL) was stirred at ambient conditions for 18 h, during which the suspension changed color from yellow to green. The suspension was filtered off, the green solid was thoroughly washed with EtOH and dried *in vacuo* at 90 °C for 8 h. Yield: 49.1 mg (92 %). Green powder. IR (neat): ν = 3029, 2214, 1699, 1594, 1496, 1003, 812, 514 cm^{-1}. Pd content (ICP-MS): 4.91 wt%.

2. Determination of Pd content

Pd concentration data were collected using an Agilent 7900 ICP-MS system (Agilent Technologies, Inc., Santa Clara, CA, USA). The instrument was equipped with quadrupole analyzer, the standard nickel interface cones, glass concentric nebulizer MicroMist (400 $\mu L \cdot min^{-1}$), the Peltier-cooled quartz spray chamber, 2.5 mm internal diameter quartz torch, low-pulsation, 10-roller peristaltic pump with three separate channels for precise delivery of samples and standards, and octopole-based collision/reaction cell (ORS4), optimized for effective and reliable removal of potential multiple polyatomic interferences using kinetic energy discrimination (KED) in helium (He) collision mode. For Pd quantification, the system provides detection limits at ppt levels and accurate results in complex and variable sample matrices.[5] The instrument was optimized using the autotuning function of the ICP-MS S4 MassHunter software. The isotopes used for the quantification of Pd with the instrument operating parameters are shown in Table S2.

Table S2. Agilent 7900 ICP-MS operating conditions.

Parameter	Setting	
ICP		
Plasma mode	General purpose	
Rf power (27 MHz) (W)	1550	
Sampling depth (mm)	10	
Plasma gas flow ($L \cdot min^{-1}$)	15	
Auxiliary gas flow ($L \cdot min^{-1}$)	0.9	
Nebulizer gas flow ($L \cdot min^{-1}$)	1.05	
Nebulizer pump (rsp)	0.1	
Spray chamber temperature (°C)	2	
Mass spectrometer	No gas mode	He mode
Extract 1 (V)	0	0
Extract 2 (V)	-205	-200
Omega bias (V)	-75	-85
Omega lens (V)	11.3	10.7
Cell entrance	-30	-40
Cell exit	-50	-60
Deflect (V)	13.8	1.6

[5] M. O. Varrà, L. Husáková, J. Patočka, S. Ghidini and E. Zanardi, Classification of transformed anchovy products based on the use of element patterns and decision trees to assess traceability and country of origin labelling, *Food Chem.*, 2021, **360**, 129790.

Plate bias	-35	-60
Helium flow (mL·min^{-1})	0	5
OctP bias	-8	-18
OctP RF	200	
Energy discrimination (V)	5	5
Isotopes (integration time, s)	^{105}Pd, ^{108}Pd, ^{103}Rh (0.1)	
Acquisition		
Points per peak	1	
Replicates	3	
Sweeps/replicate	100	

Analyte concentrations were determined with external calibration ranging from blank to 100 µg·L^{-1} of Pd. Calibration standards were premixed daily from 500 mg·L^{-1} of Pd stock solution prepared by an appropriate dilution of the SCP Science standard (1 g·L^{-1}) using 1% HNO_3 to ensure the stability of the analyte. Linear calibrations were obtained with coefficients of determination > 0.999 to compensate for possible instrumental drift and matrix effects, a 200 µg·L^{-1} Rh internal standard element (SCP Science, Canada) was simultaneously aspired and mixed with samples.

Samples were digested in a Speedwave XPERT closed microwave oven system (Berghof, Eningen, Germany) with a power output of dual magnetrons of 2×1.000 W and optical sensors for contactless real-time recording of the sample temperature and pressure in each vessel. The high-pressure resistant S5 (up to 100 bar) TFM™-PTFE vessels DAK100 were used for sample digestion. The 3–10 mg sample aliquots were accurately weighed in PTFE vessels, then 6 mL of 65% HNO_3 was added. The vessels were closed, and the following microwave oven heating program was performed: (i) 5 min at 170 °C and 60 % power (ramp 5 min), (ii) 25 min at 220 °C and 70 % power (ramp 5 min), (iii) 5 min at 100 °C and 10 % power (ramp 1 min). After digestion, the solutions were cooled to room temperature and diluted to 25 mL with deionized water. The digests were diluted 100× with deionized water prior to analysis by ICP-MS. A liquid sample was analyzed directly after appropriate dilution with deionized water. Each sample was prepared in four replicates. Blanks consisting of deionized water and reagents were subjected to a similar preparation procedure.

3. NMR Spectra

The ^{1}H, ^{13}C, and ^{13}C CP/MAS NMR spectra were measured at 25 °C on a Bruker Ascend™ instrument at 500/125 MHz equipped either with a nitrogen-cooled cryoprobe or a 3.2 mm MAS probe. The solution ^{1}H and ^{13}C NMR spectra were measured in $CDCl_3$ or DMSO-d_6. The chemical shifts are given in ppm relative to the Me_4Si signal. The residual solvent signal was used as an internal standard ($CDCl_3$: 7.24 and 77.23 ppm, DMSO-d_6: 2.50 and 39.51 ppm for ^{1}H and ^{13}C NMR spectra, respectively). The observed signals are described as *s* (singlet) and *m* (multiplet). The solid-state ^{13}C CP/MAS NMR spectra were acquired at a spinning rate of 5 kHz, with a pulse length of 2.4 μs, a contact time of 2 ms, and a recycle delay of 1.5 s. No reference standard was used.

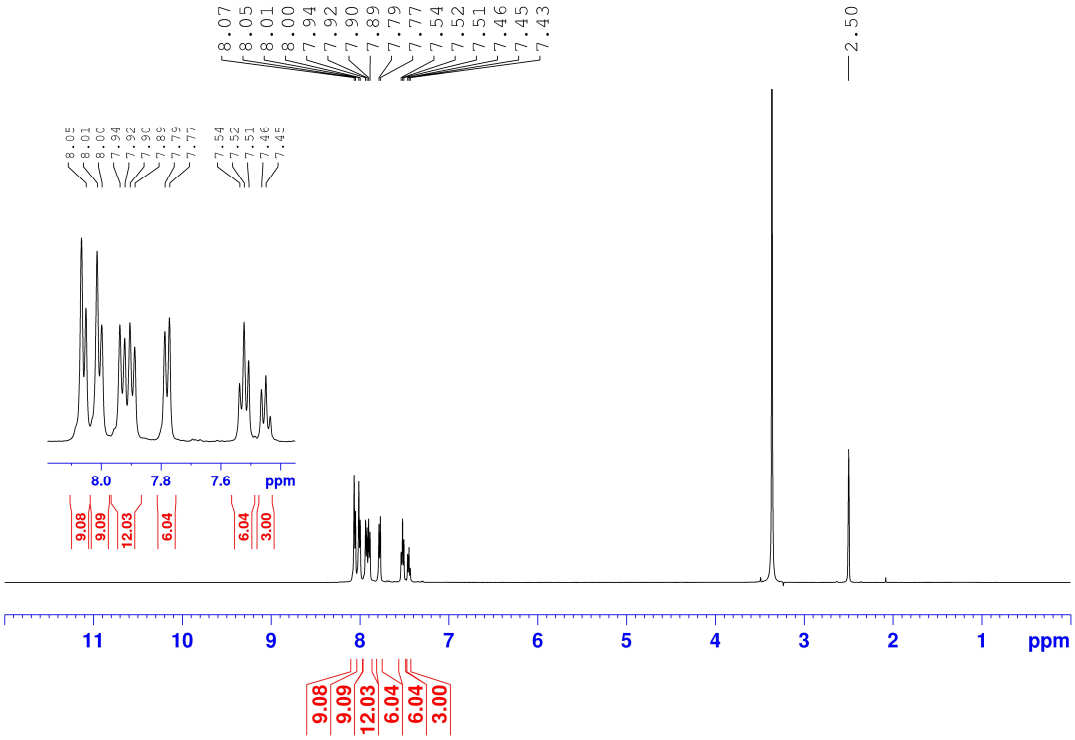

Figure S1. ^{1}H NMR (500 MHz, DMSO-d_6, 25 °C) spectrum of **MC**.

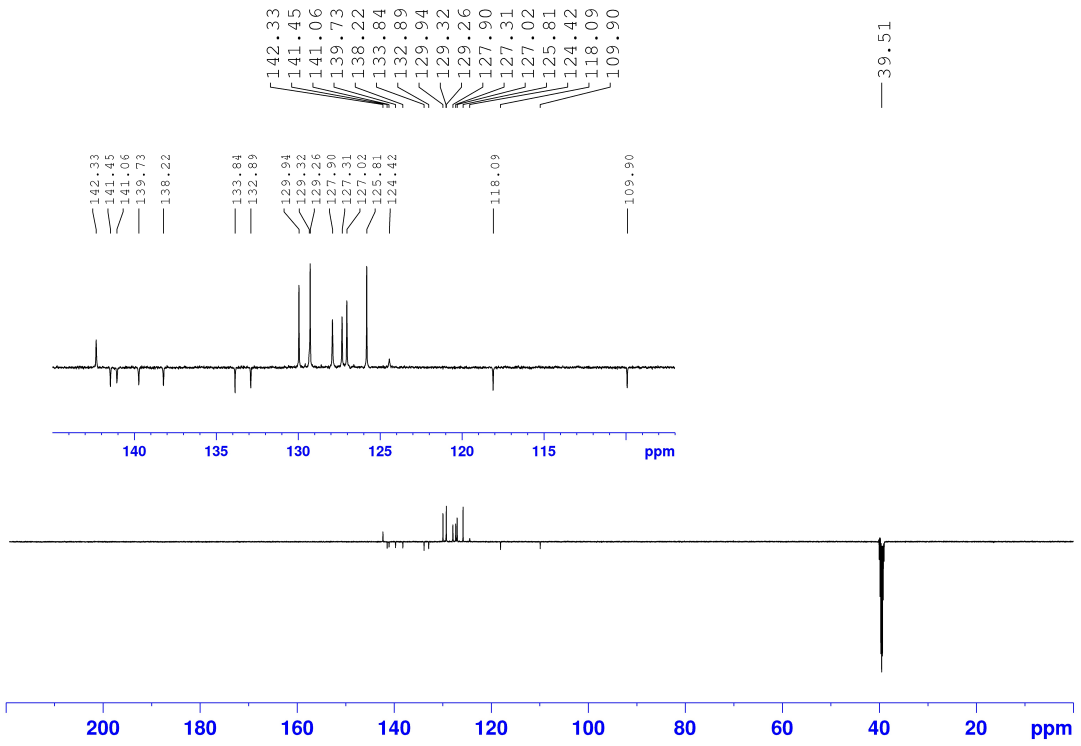

Figure S2. ^{13}C NMR (125 MHz, DMSO-d_6, 25 °C) spectrum of **MC**.

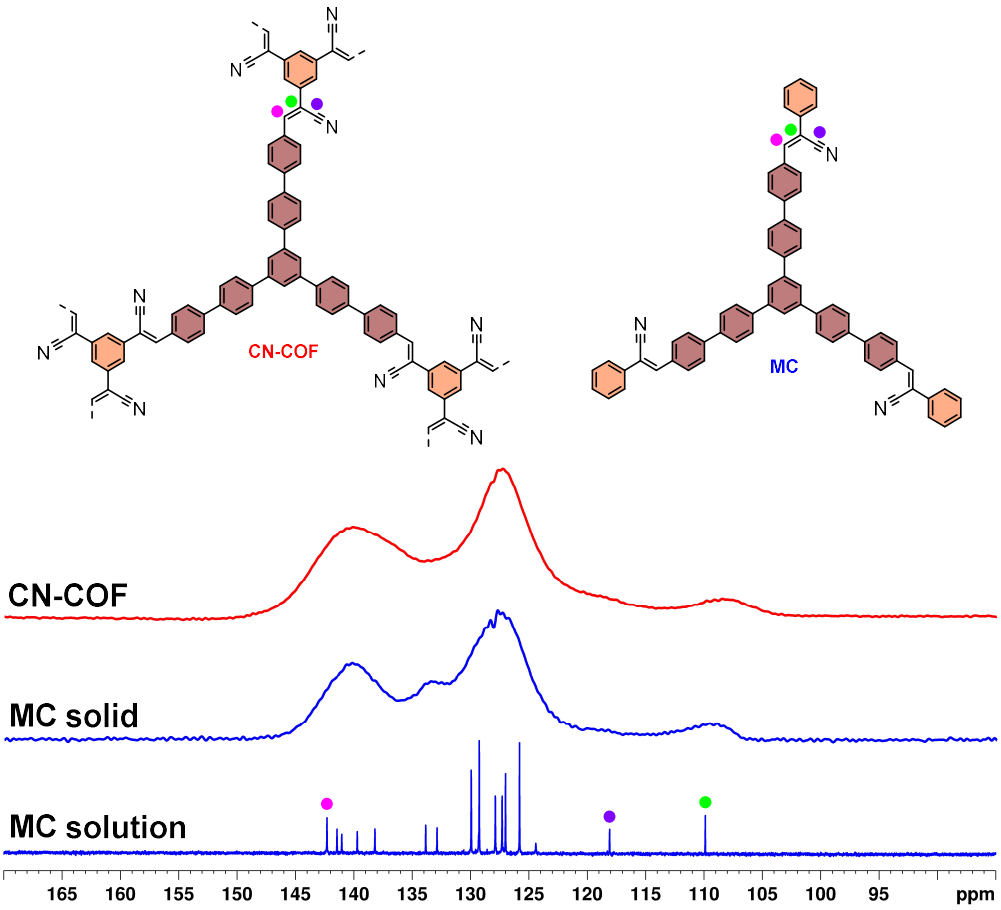

Figure S3. ^{13}C CP/MAS NMR (125 MHz, 25 °C) spectra of **CN-COF** and **MC** along with ^{13}C NMR (125 MHz, 25 °C) spectrum of **MC** in DMSO-d_6.

4. HR-FT-MALDI-MS

The high-resolution mass spectra were measured by the dried droplet method using a MALDI mass spectrometer LTQ Orbitrap XL (Thermo Fisher Scientific) equipped with a nitrogen UV laser (337 nm, 60 Hz). The spectra were measured in the positive mode in normal mass range with a resolution of 100 000 at *m/z* = 400. DCTB was used as a matrix.

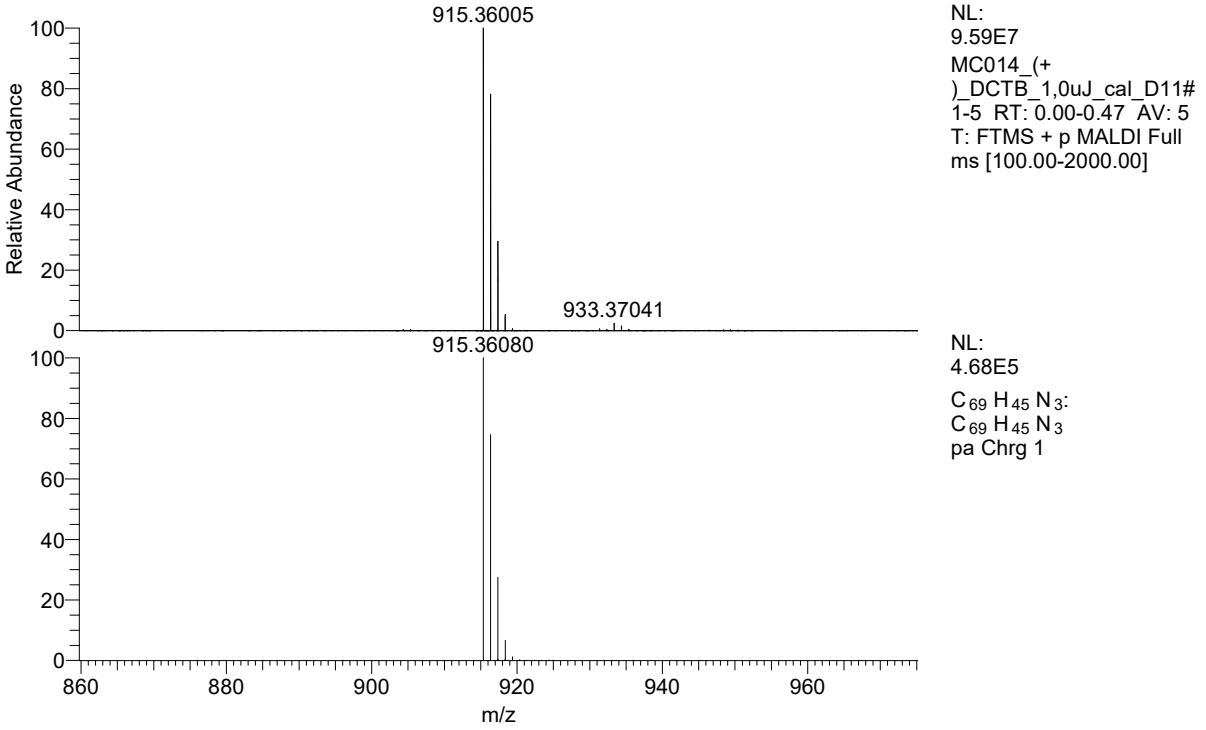

Figure S4. HR-FT-MALDI-MS spectrum of **MC** ($[M]^+$ = 915.36080 Da). Top measured and bottom predicted spectrum.

5. FT-IR and Raman Spectra

The FT-IR and Raman spectra were recorded on a Thermo Scientific Nicolet iS50 spectrometer equipped with integrated iS50 ATR and iS50 Raman modules (1064 nm diode laser, InGaAs detector) using neat samples. Raman measurements were performed using a motorized XYZ stage with autofocus.

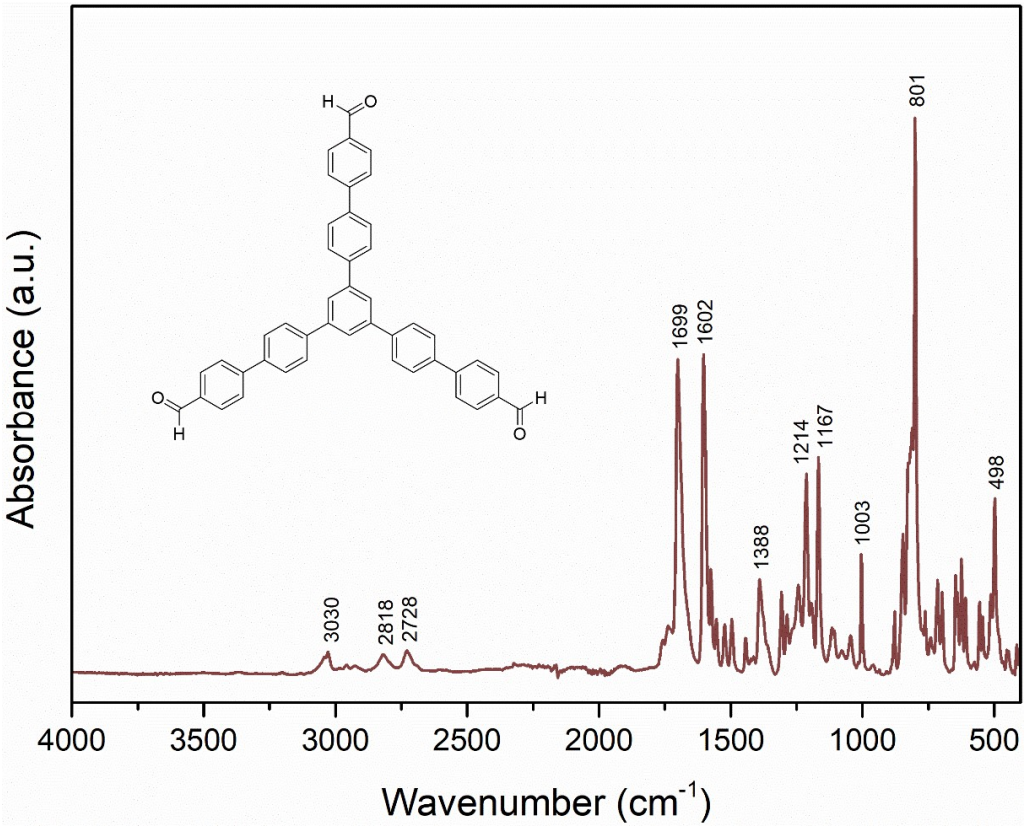

Figure S5. FT-IR (neat) spectrum of **TFBB**.

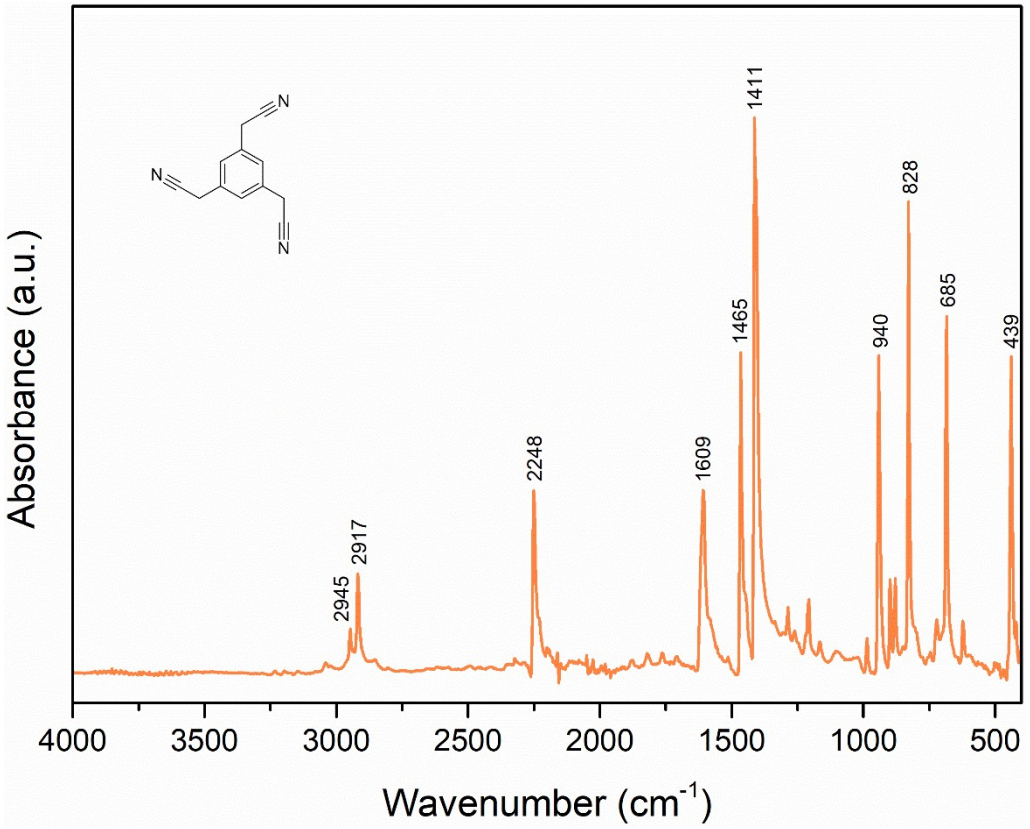

Figure S6. FT-IR (neat) spectrum of **BTAN**.

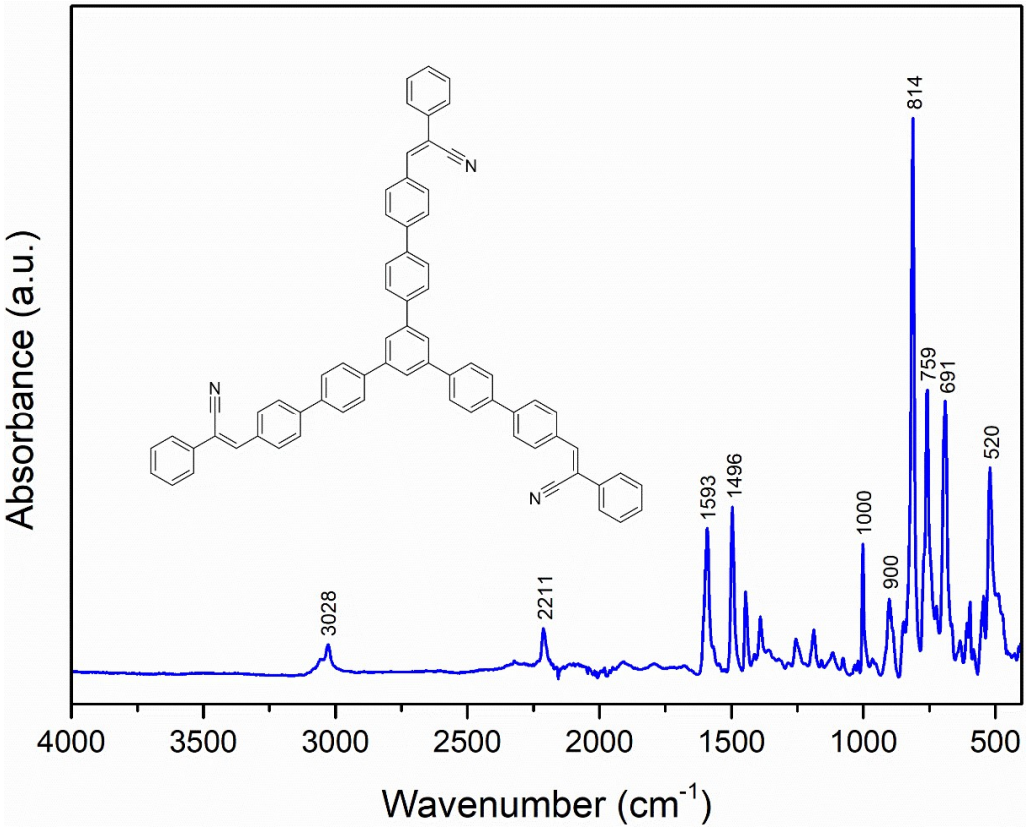

Figure S7. FT-IR (neat) spectrum of **MC**.

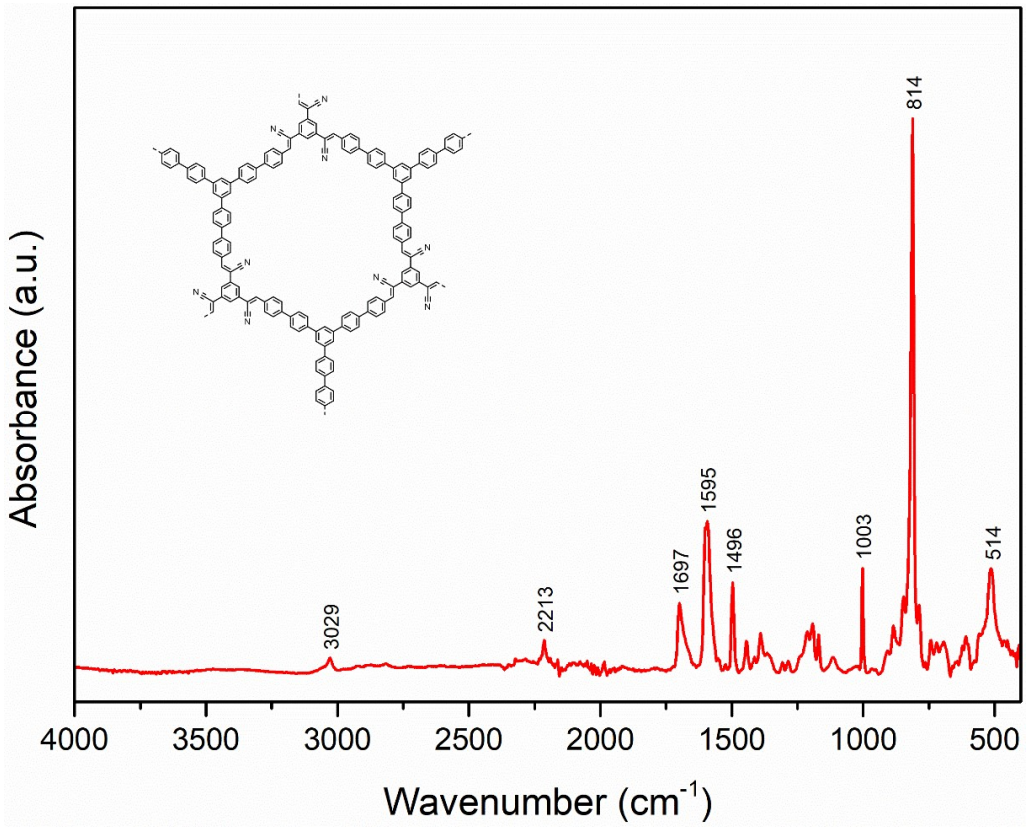

Figure S8. FT-IR (neat) spectrum of **CN-COF**.

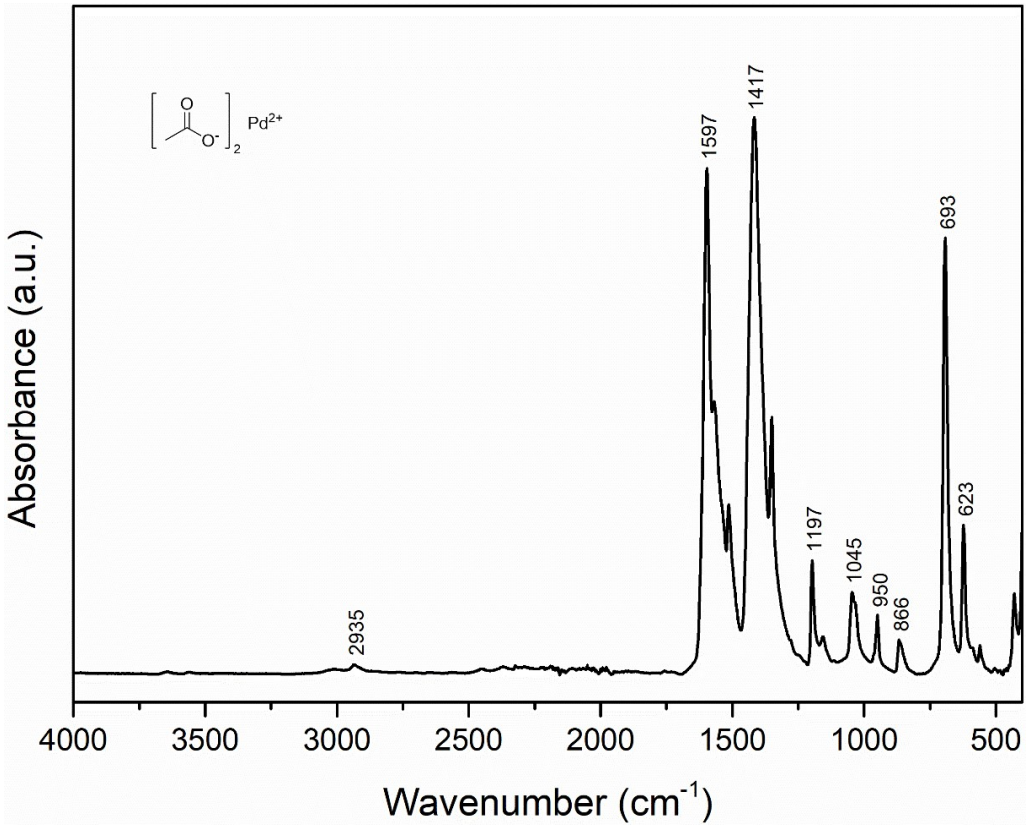

Figure S9. FT-IR (neat) spectrum of $Pd(OAc)_2$.

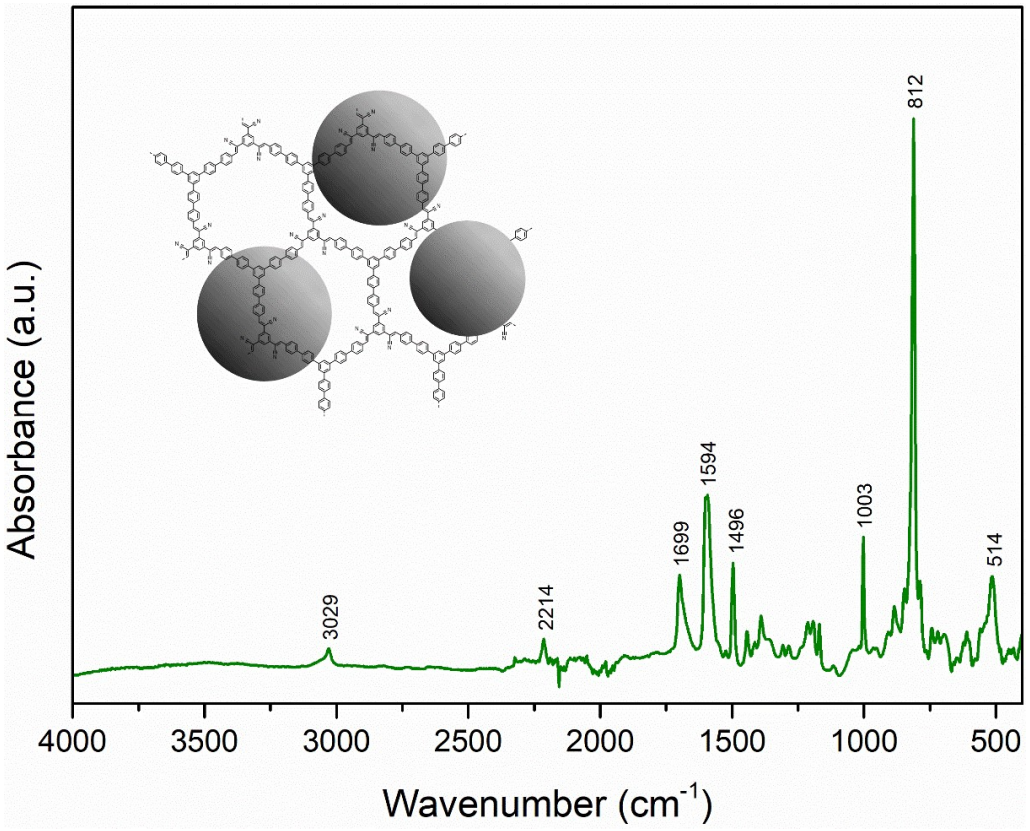

Figure S10. FT-IR (neat) spectrum of **Pd@CN-COF**.

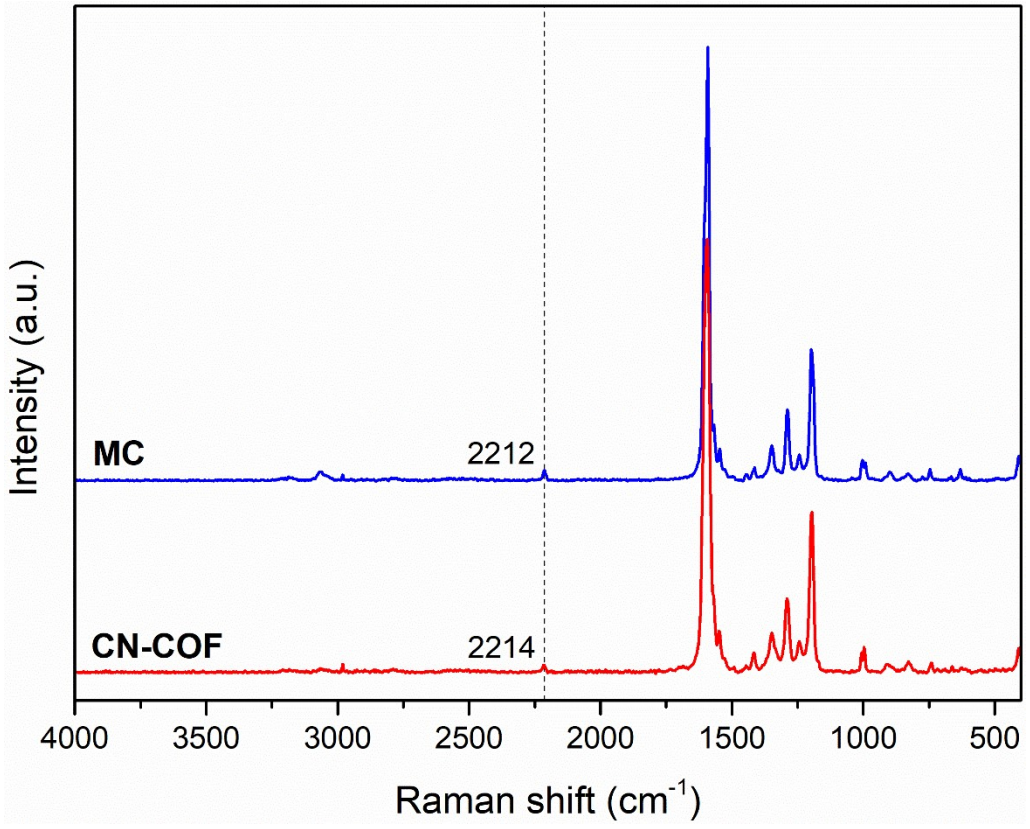

Figure S11. Raman spectra of **MC** and **CN-COF**.

6. Structural Simulation

Structural models of **CN-COF** were built using a force field method and further optimized with DFTB, both as implemented in the Amsterdam Modeling Suite (AMS 2023.104) software.[6] The unit cell parameters were determined as *a* = *b* = 26.2656 Å, *c* = 7.2024 Å, α = β = 90°, γ = 120° and *a* = *b* = 26.1976 Å, *c* = 6.5951 Å, α = β = 90°, γ = 120° for AA and AB stacking, respectively. The electron density distribution was obtained from periodic DFT calculations (BAND), employing the BLYP-D3 functional and a DZ basis set.

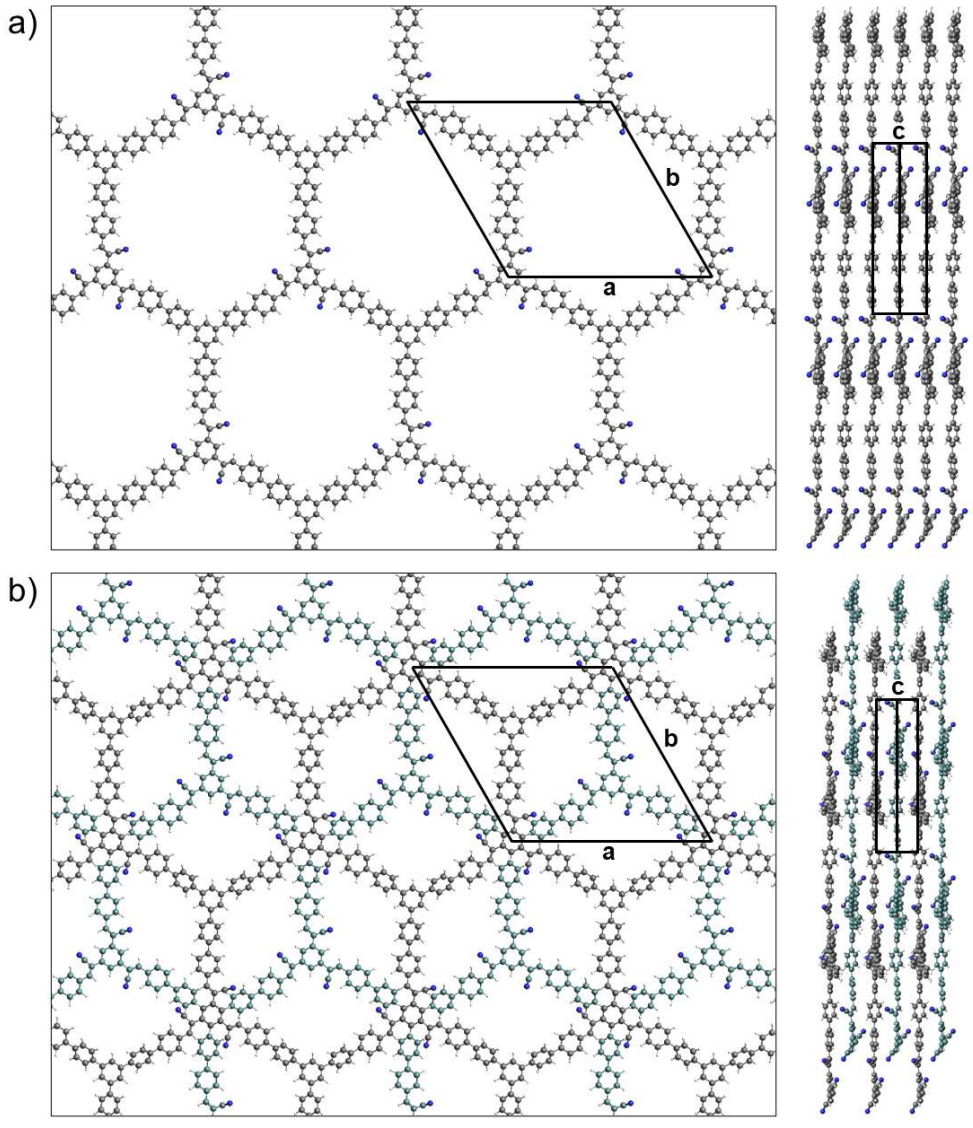

Figure S12. Top and side views of the simulated structures of AA (a) and AB stacking (b) in **CN-COF**.

[6] AMS 2023.104, SCM, Theoretical Chemistry, Vrije Universiteit, Amsterdam, The Netherlands, http://www.scm.com.

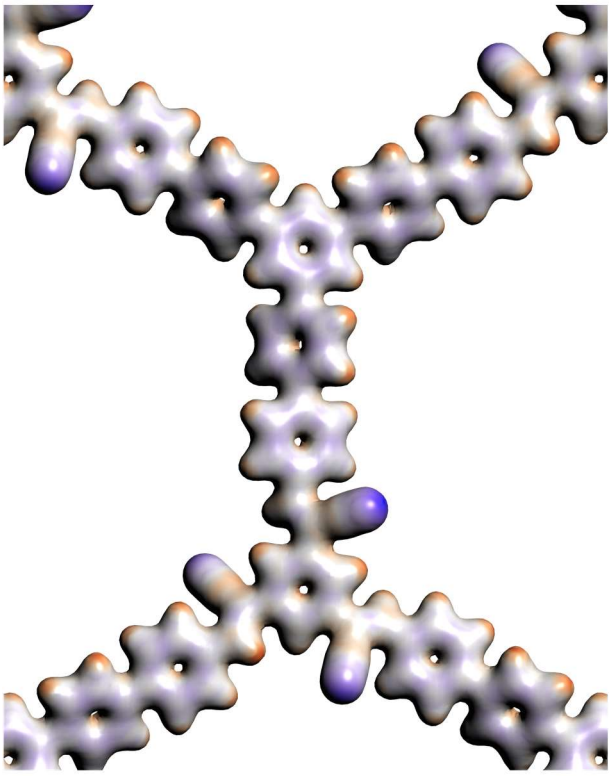

Figure S13. Calculated electron density distribution within **CN-COF** (AA stacking).

7. Powder X-ray Diffraction Analysis

The PXRD measurements were collected at room temperature on a tabletop Rigaku MiniFlex 600 diffractometer with a graphite monochromator and a silicon strip detector D/teX Ultra using the CuKα radiation (λ = 1.5418 Å, U = 40 kV, I = 15 mA). The experiments were performed in the Bragg-Brentano parafocusing geometry over a range of 2.5–90° 2θ with a step size of 0.02° and a scan rate of 5°/min. The samples were finely ground and pressed onto flat glass sample holders (the depth of the sample layer 0,2–0.5 mm).

The obtained PXRD diffractogram (Figure S14 for the original pattern and Figure S15 after the background subtraction) was optimized with the help of the Jana2006 software[7] by employing the Le Bail refinement procedure. The refinement was performed with fixed lattice parameters (a = b = 26.2656 Å, c = 7.2024 Å, α = β = 90°, γ = 120°), previously obtained from the molecular simulations for the AA stacking mode, while optimizing the sample displacement parameter. The optimization was performed in the range of 2.5–35° 2θ. The background was modeled with the Legendre polynomial (number of terms = 7), and the peak shape was modeled by the Lorentz function. The peak asymmetry was not corrected. The fit of the experimental data was generally very good (GOF = 1.24, R_p = 1.67 %, R_{wp} = 2.27 %).

[7] V. Petříček, M. Dušek and L. Palatinus, Crystallographic Computing System JANA2006: General features, *Z. Kristallogr. Cryst. Mater.*, 2014, **229**, 345–352.

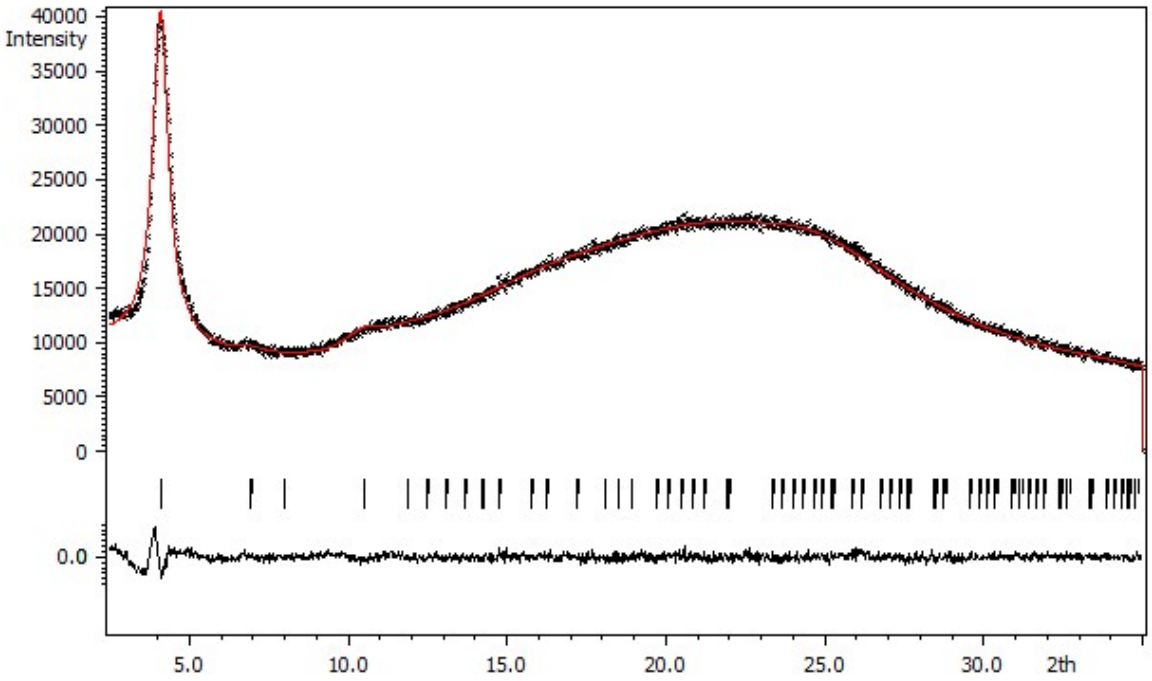

Figure S14. The as-measured PXRD diffractogram of the **CN-COF** fitted by the Le Bail refinement.

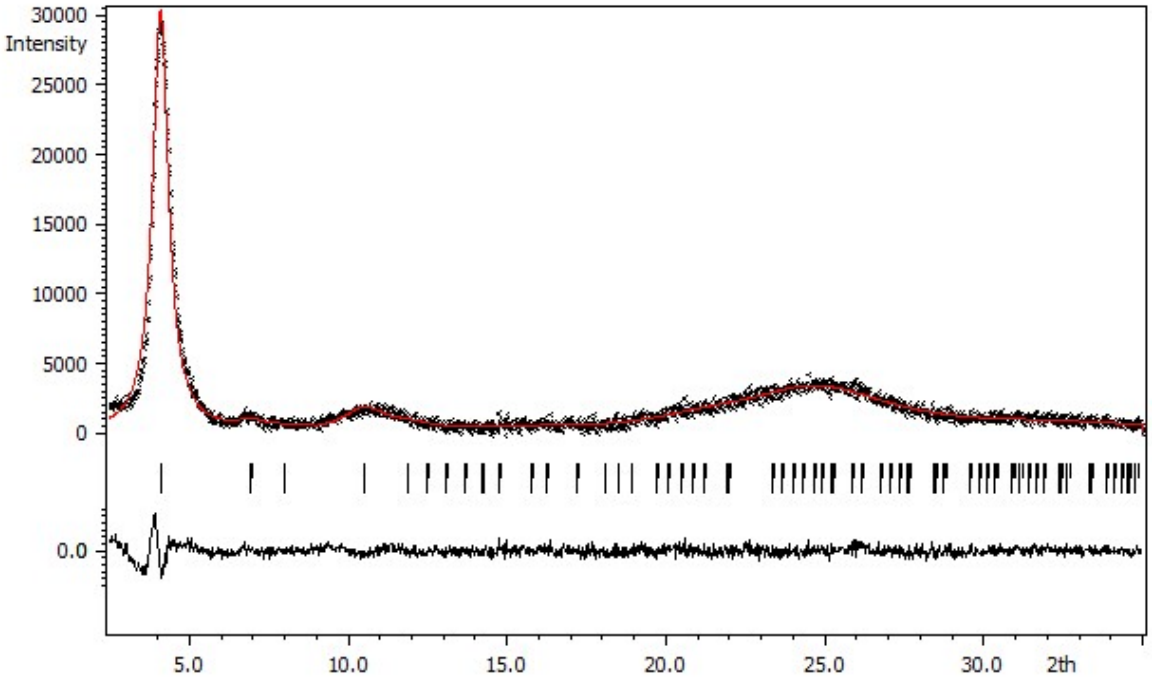

Figure S15. The PXRD diffractogram of **CN-COF** after the subtraction of the background, fitted by the Le Bail refinement.

8. Microscopic Techniques

The SEM images were acquired using a JEOL JSM-7500F field-emission scanning electron microscope (FE-SEM). Prior to analysis, the **CN-COF** sample was coated with a 5 nm layer of carbon to enhance conductivity. The resulting images were formed by mixing signals from secondary (SE) and backscattered (BSE) electrons using an r-filter. The nanoparticle sizes were measured using the Nanomeasure software.

The morphology, structure, and chemical composition of **CN-COF** were investigated using a Cs image-corrected transmission electron microscope (TITAN Themis 60–300 Cubed, Thermo Fisher Scientific, USA). High-resolution TEM imaging was performed at an accelerating voltage of 300 kV. Scanning TEM-energy dispersive X-ray spectroscopy (STEM-EDX) elemental mapping was conducted at both 300 kV and 60 kV. STEM-EDX analysis was carried out using a Super-X detector, and the elemental maps and compositional data were acquired and processed using Velox software, employing the standard Cliff–Lorimer (K-factor) quantification method. Sample for TEM analysis consisted of bulk powdered material that was either dispersed in pure methanol and drop-cast onto copper TEM grids coated with a holey carbon membrane or applied directly to the grids.

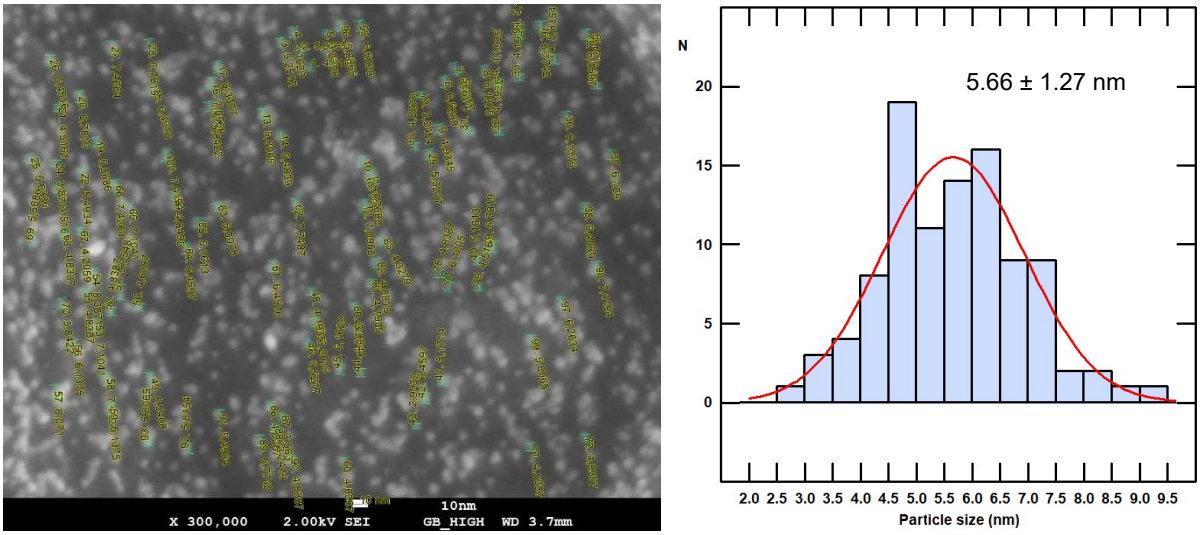

Figure S16. SEM image analysis of **Pd@CN-COF** (left) with the histogram of particle size distribution (right).

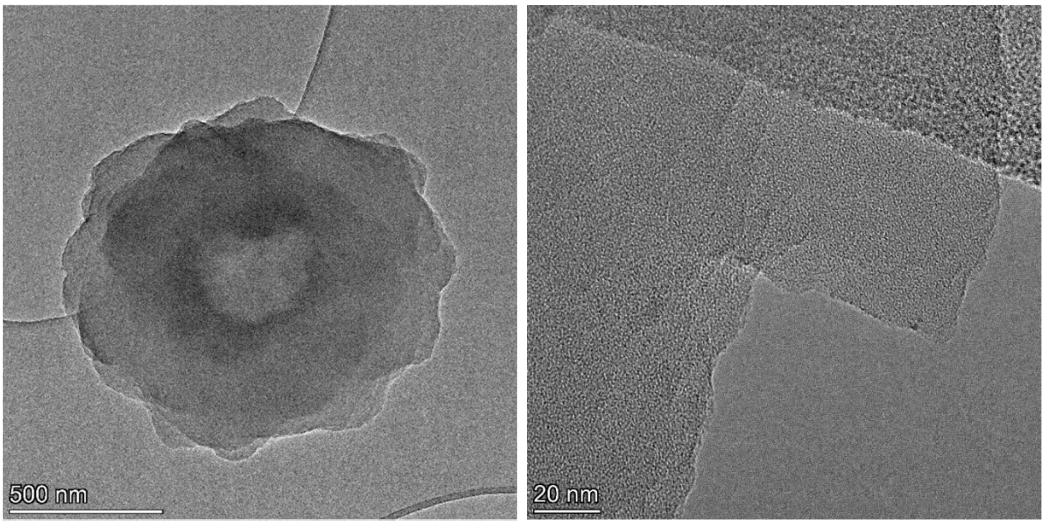

Figure S17. HR-TEM characterization of **CN-COF**.

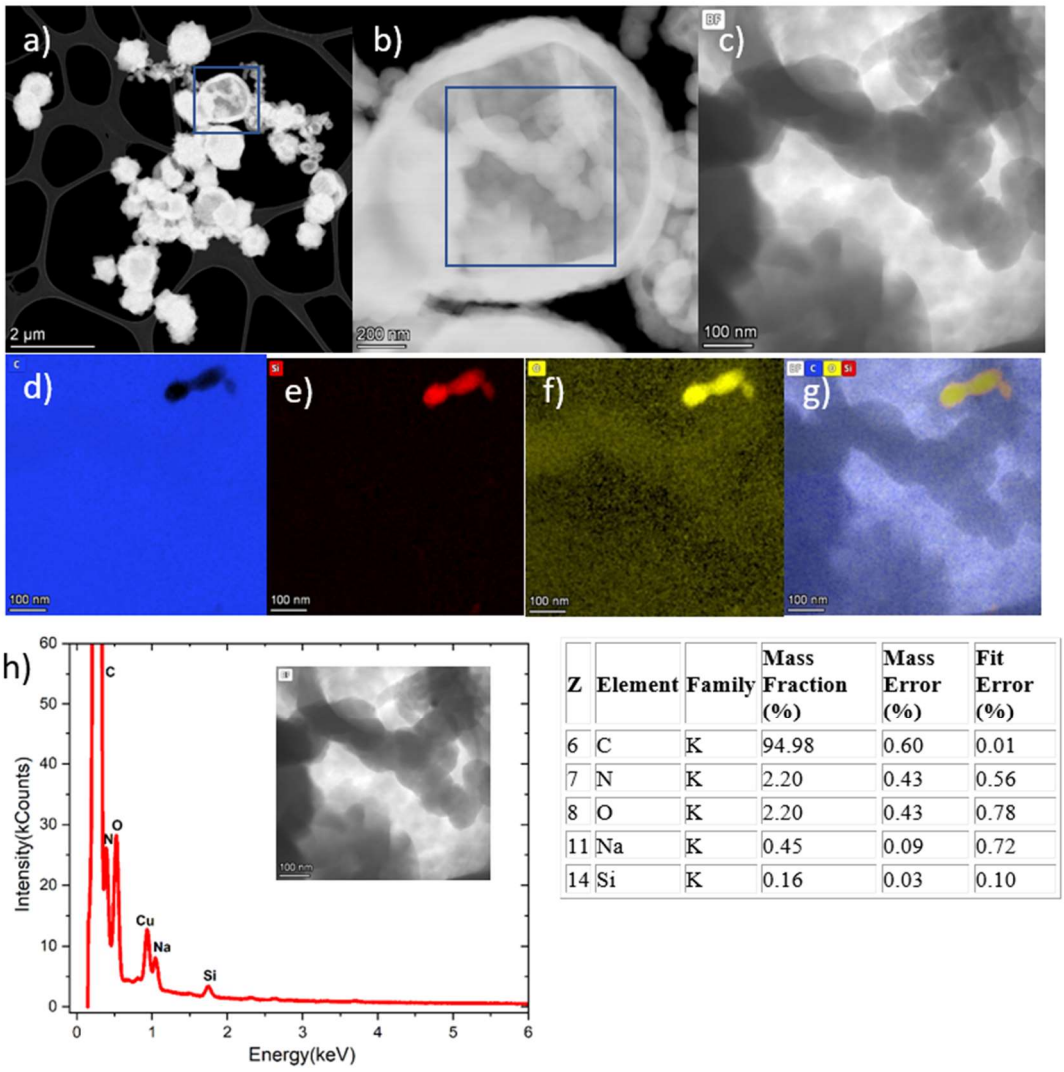

Z	Element	Family	Mass Fraction (%)	Mass Error (%)	Fit Error (%)
6	C	K	94.98	0.60	0.01
7	N	K	2.20	0.43	0.56
8	O	K	2.20	0.43	0.78
11	Na	K	0.45	0.09	0.72
14	Si	K	0.16	0.03	0.10

Figure S13. STEM-EDX characterization of **CN-COF** particles: (a,b) HAADF-STEM images; (c) BF-STEM image; (d–f) elemental maps for C-K, Si-K, and O-K; (g) overlay map; (h) EDX spectrum with elemental composition in mass fractions.

9. X-ray Photoelectron Spectroscopy

The surface chemical compositions of **CN-COF** and **Pd@CN-COF** were assessed by XPS using a Scienta-Omicron ESCA 2SR instrument, with an Al-Kα monochromatic X-ray source (hν = 1486.69 eV) operated at 200 W and 12.5 kV. The compensation of the surface charge of the samples was controlled with an electron gun (CN 10) operated at 7 μA and 2.0 eV. The acquired spectra were further fitted using CasaXPS software and referenced to the C=C species in the C 1s signal at 284.5 eV, in order to perform the binding energy scale correction. Fitting of the C 1s and N 1s high-resolution spectra was done using a mixed Shirley-type background and mixed Gaussian-Lorentzian functions GL (30). Pd 3d spectrum was fitted with Shirley-type background and asymmetric Lorentzian function LA (0.95, 2, 150) for metallic state (Pd^0) and mixed Gaussian-Lorentzian functions GL (30) for Pd oxides/hydroxides and Pd plasmon loss. The area ratio and binding energy distance constraints for the spin-orbit splitting, Pd $3d_{5/2}$ and Pd $3d_{3/2}$, 3:2 and 5.26 eV were considered.

The surface chemical composition of **CN-COF** and **Pd@CN-COF** revealed the signals of C, O, N, Na, and Pd in the corresponding survey spectra (Figure S19a). The C and N signals originate from the intrinsic nature of the support; however, some parts of the C signal are derived from adventitious carbon, as well as O, which is highly associated with the latter and with the interaction with Pd. Na arises from the NaOH used during the synthesis of **CN-COF**, and Pd signal confirms the presence of this element in **Pd@CN-COF**. The C 1s high-resolution spectra of both **CN-COF** and **Pd@CN-COF** were peak fitted using seven components (Figure S19b). The first signal at 284.5 eV was attributed to the presence of C=C[8] from the **CN-COF** structure. At 285.0 eV, the adventitious carbon C–(C,H) appears.[9] The carbon bonded with nitrogen, C–N (C≡N), appears at 286.0 eV.[9,10] The carbon single bonded with oxygen C–O at 286.8 eV[9] and carbon double bonded with oxygen C=O, is recorded at 288.2 eV,[9] while COOH appeared at 289.4 eV.[9] The last C contribution at 291.2 eV corresponds to π-π^*

[8] R. Tao, B. Feng, C. Wang, H. Zhang, R. Chen, K. Li, J. Xi, X. Deng, J. Li and Y. Yang, Feasible preparation of preferentially oriented (111) Pd nanocrystals supported on cyano-COFs for ultrahigh activity in C–C cross-couplings, *J. Catal.*, 2024, **432**, 115399.
[9] P. G. Rouxhet and M. J. Genet, XPS analysis of bio-organic systems, *Surf. Interface Anal.*, 2011, **43**, 1453–1470.
[10] J. F. Moulder, W. F. Stickle, P. E. Sobol and K. D. Bomben, *Handbook of X-ray Photoelectron Spectroscopy*; Physical Electronics, Inc.: Eden Prairie, Minnesota, 1995; pp. 43, 227.

shake-up satellite.[11] The N 1s spectra (Figure S19c) in both cases show one chemical species, C–N (C≡N) at ~399.5 eV,[10] however, there is a small shift of 0.2 eV towards lower binding energy when the Pd is added into the structure, demonstrating a clear perturbation of the electronic cloud of the nitrile groups due to the Pd atoms. The Pd 3d XPS spectra (Figure S19d) show the corresponding spin-orbit splitting Pd $3d_{5/2}$/Pd $3d_{3/2}$. Seven components were used to perform the peak fitting; six of them are associated with the spin-orbit splitting, which corresponds to three different chemical species, and the last one is associated with the characteristic plasmon loss that appears when the Pd is mostly metallic. The first couple (red) are located at 335.3/340.6 eV, confirming the presence of Pd in a metallic state (Pd^0).[12,13] The second doublet (blue) centered at 336.8/342.1 eV is related to Pd^{2+},[12,14] while the third doublet (green) at 338.4/343.7 eV is assigned to Pd^{4+},[15] Pd^{2+} and Pd^{4+} are likely related to the corresponding oxides or hydroxides. The surface atomic concentration of each Pd species in **Pd@CN-COF** was also determined, with the contents of Pd^0, Pd^{2+}, and Pd^{4+} being 71.7 at%, 20.1 at%, and 8.2 at%, respectively. These results indicate that the surface amount of the metallic Pd is 2.5 times higher than that of its combined counterparts.

[11] M. C. Biesinger, Accessing the robustness of adventitious carbon for charge referencing (correction) purposes in XPS analysis: Insights from a multi-user facility data review, *Appl. Surf. Sci.*, 2022, **597**, 153681.

[12] B. Bawab, S. M. Thalluri, J. Rodriguez-Pereira, H. Sopha, R. Zazpe and J. M. Macak, Anodic TiO_2 nanotube layers decorated by Pd nanoparticles using ALD: An efficient electrocatalyst from methanol oxidation, *Electrochim. Acta*, 2022, **429**, 141044.

[13] C. M. Schott, J. Holl, R. Zazpe, M. Kopp, O. Man, S. M. Thalluri, J. Rodriguez-Pereira, P. M. Schneider, K.-T. Song, E. Keles, P. Peljo, J. J. Jasielec, E. L. Gubanova, J. M. Macak and A. S. Bandarenka, Revealing Catalytic Properties of Palladium/Gold Systems toward Hydrogen Evolution, Oxidation, and Absorption with Scanning Electrochemical Microscopy, *ACS Catal.*, 2025, **15**, 9035–9046.

[14] T. L. Barr, Recent advances in x-ray photoelectron spectroscopy studies of oxides, *J. Vac. Sci. Technol. A*, 1991, **9**, 1793–1805.

[15] B. Bawab, S. M. Thalluri, E. Kolíbalová, R. Zazpe, L. Jelínek, J. Rodriguez-Pereira and J. M. Macak, Synergistic effect of Pd single atoms and nanoparticles deposited on carbon supports by ALD boosts alkaline hydrogen evolution reaction, *J. Chem. Eng.*, 2024, **482**, 148959.

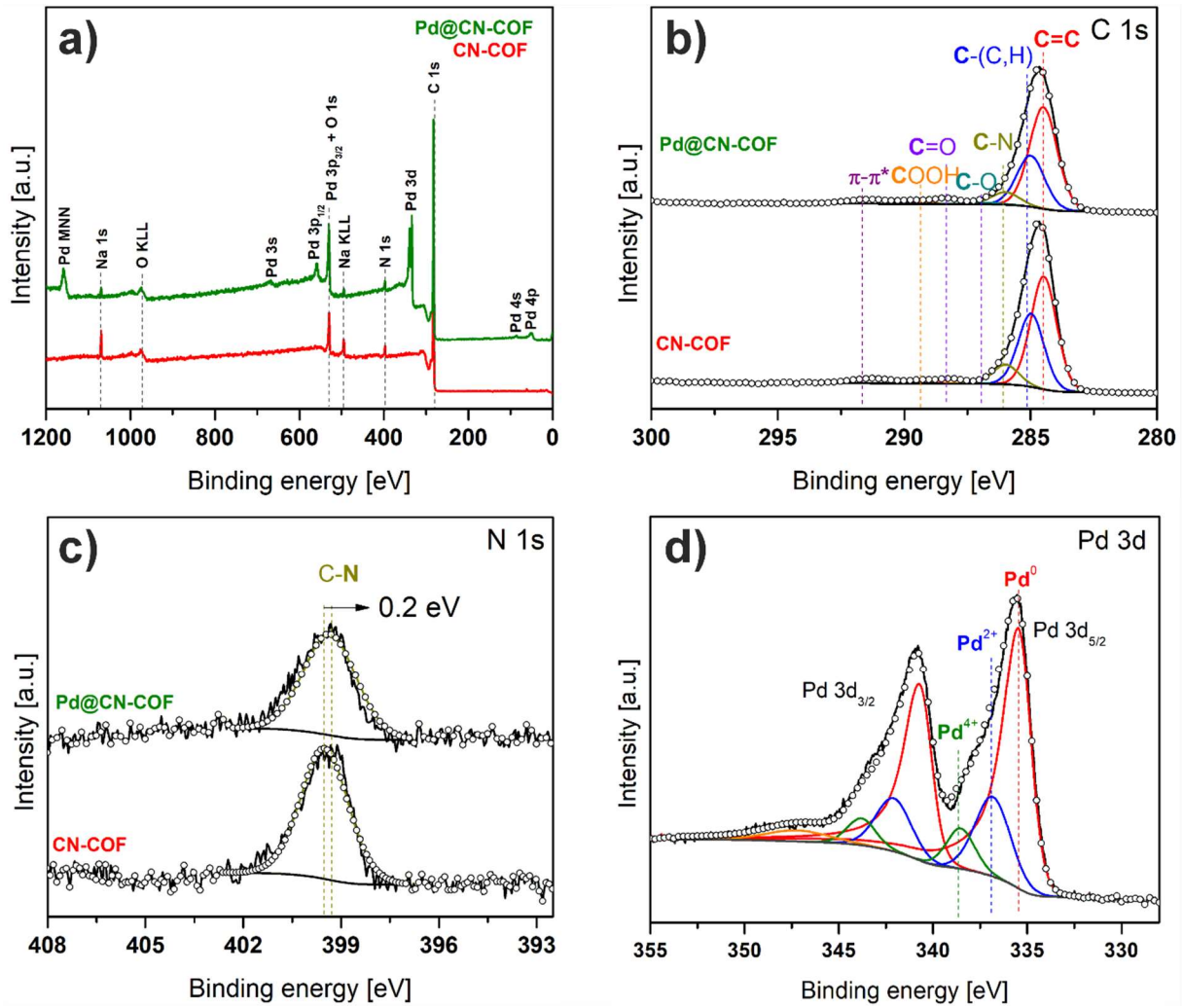

Figure S19. XPS spectra of **CN-COF** and **Pd@CN-COF**. The survey spectra (a), high-resolution spectra of C 1s (b), N 1s (c), and Pd 3d (d).

10. Thermal Properties

Thermal properties were measured by thermogravimetric analysis (TGA) and differential scanning calorimetry (DSC). TGA was measured in open alumina crucibles under N_2 inert atmosphere (50 mL·min^{-1}) with a scanning rate of 5 °C/min within the range 25–1000 °C. The TGA measurements were carried out using a Mettler-Toledo STAR^e System TGA 2 equipped with a horizontal furnace LF (400 W, 1100 °C), balance XP5 (resolution 1 μg) and cooling system HUBER Minichiller 600. The initial sample weight was approximately 7 mg. DSC was measured in aluminous crucibles sealed with a pierced lid under N_2 inert atmosphere (60 mL·min^{-1}) with a scanning rate of 5 °C/min within the range 25–600 °C. The DSC measurements were carried out using Mettler-Toledo STAR^e System DSC 2/700 equipped with FRS 6 ceramic sensor and cooling system HUBER TC100-MT RC 23.

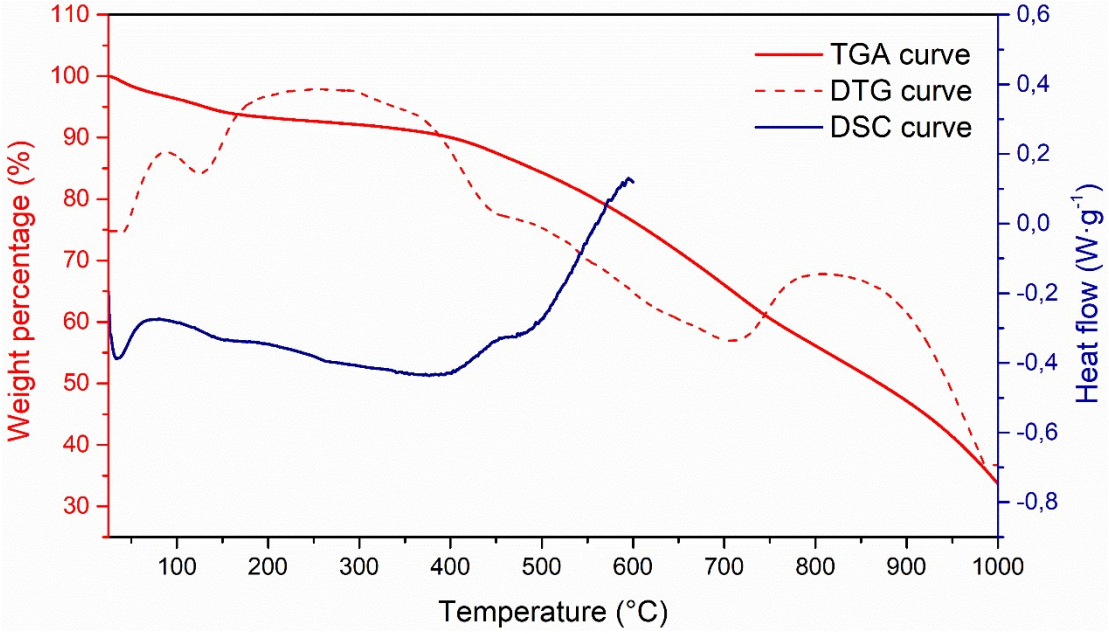

Figure S20. TGA, DTG, and DSC profiles of **CN-COF**.

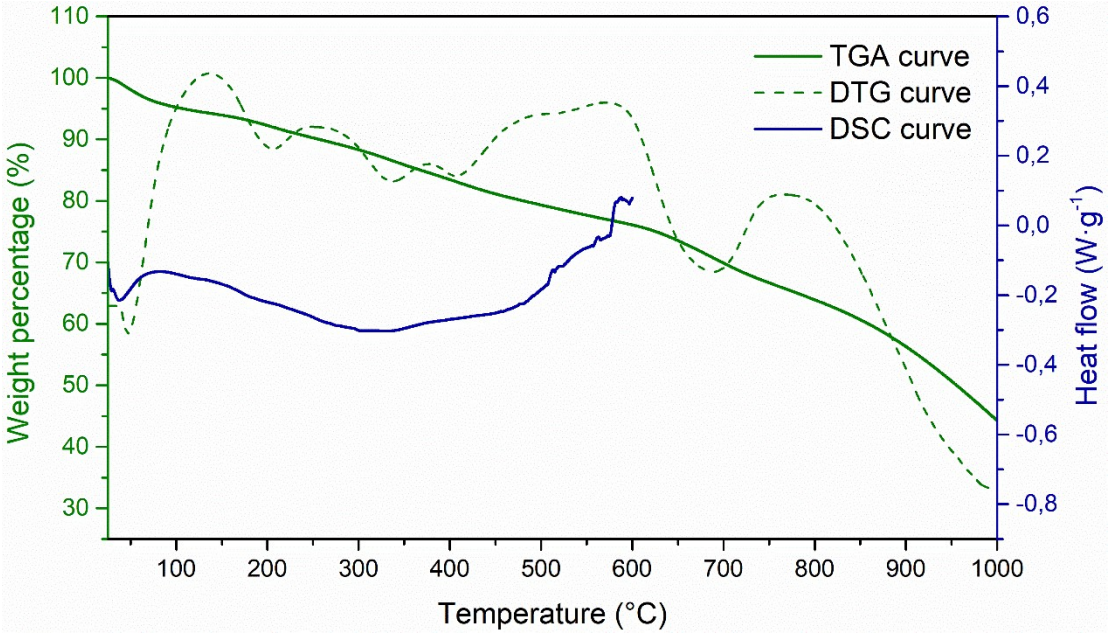

Figure S21. TGA, DTG, and DSC profiles of **Pd@CN-COF**.

11. Volumetry

The textural properties of **CN-COF** and **Pd@CN-COF** were investigated using physical adsorption of nitrogen. Prior to measurement, the material (ca. 50 mg) was degassed by gradual slow heating (0.5 °C/min) up to 110 °C in a dynamic vacuum of a turbomolecular pump (vacuum better than 10^{-3} Torr). At the target temperature, the sample was evacuated for 10 h. N_2 (purity 99.9999%) adsorption isotherm was measured using an automatic volumetric apparatus ASAP 2020 (Micromeritics, USA) at liquid nitrogen temperature. The free volume was determined using helium (purity 99.9999 %). The adsorption equilibrium threshold was set as a < 0.01 % pressure change on a 5-second interval. The saturated nitrogen vapor pressure was automatically measured every 5 h in a separate saturation tube during the experiment. The measured data were subsequently evaluated using MicroActive data reduction software (Micromeritics, USA). The specific surface area was evaluated from nitrogen adsorption isotherms by B.E.T. theory applied to the data in an interval of relative pressures satisfying the condition of the positive derivation of the data in the so-called Rouquerol plot ($n_{ads}(1-P/P_0)$ vs P/P_0 dependence).[16] Micropore volume (V_μ) and external surface area (S_{ext}), thus surface area not associated with ultramicropores, were calculated from a modified non-linear BET isotherm (fixed P/P_0 = 0.01–0.35 interval) with a volume of micropores as the third parameter.[17] The mesopore size was determined using the BJH approach and the thickness curve of Carbon Black STSA, with the understanding that the model does not fully correspond to the real material, but a better one is not available.

The N_2 adsorption isotherms of parent **CN-COF** and **Pd@CN-COF** catalyst in Figure S22A show a shape characteristic of type I(b) according to the IUPAC classification,[18] which represents materials having a wider distribution of micropore sizes and extending into the region of small mesopores (ca. up to 2.5 nm). Surprisingly, the Pd-catalyst exhibits a specific surface area slightly larger (358 $m^2 \cdot g^{-1}$) than the parent COF (258 $m^2 \cdot g^{-1}$). Total pore volume is 0.186 and 0.225 $cm^3 \cdot g^{-1}$ for parent

[16] J. Rouquerol, P. Llewellyn and F. Rouquerol, Is the bet equation applicable to microporous adsorbents?, *Stud. Surf. Sci. Catal.*, 2007, **160**, 49–56.
[17] P. Schneider, Adsorption isotherms of microporous-mesoporous solids revisited, *Appl. Catal. A Gen.*, 1995, **129**, 157–165.
[18] M. Thommes, K. Kaneko, A. V. Neimark, J. P. Olivier, F. Rodriguez-Reinoso, J. Rouquerol, K. S. W. Sing, Physisorption of gases, with special reference to the evaluation of surface area and pore size distribution (IUPAC Technical Report), *Pure Appl. Chem.*, 2015, **87**, 1051–1069.

CN-COF and **Pd@CN-COF** catalyst, respectively. Fitting the data in the interval P/P_0 = 0.01–0.3 with a modified, three-parameter, B.E.T. equation demonstrated an insignificant contribution of ultramicropores to the material porosity in both materials. The size distribution of the mesopores evaluated by the BHJ approach manifested the absence of mesopores in the catalyst (Figure S22B).

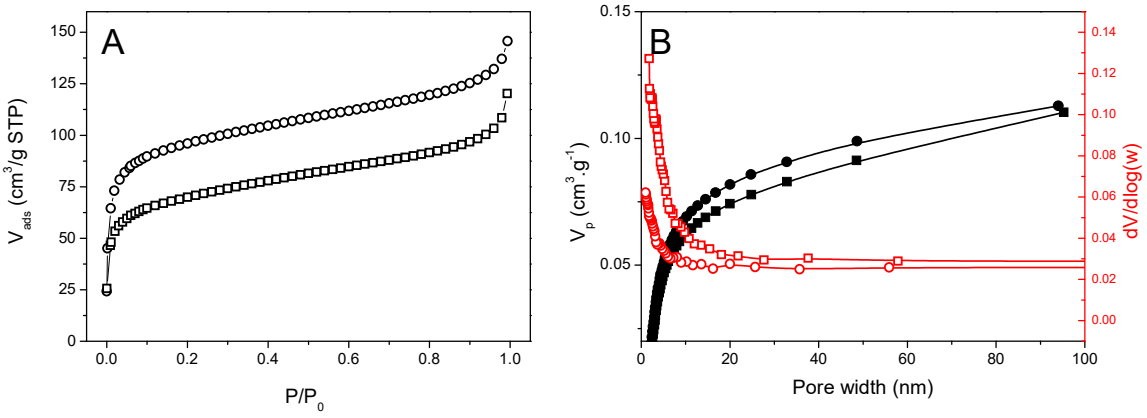

Figure S22. N_2 adsorption isotherm of parent **CN-COF** (squares) and **Pd@CN-COF** (circles) catalyst at 77 K (A) and cumulative pore volume (black) and mesopore size distribution (red) calculated from the adsorption branch of the isotherm by BJH methodology employing Carbon Black STSA thickness curve (B).

Information on the dispersion of Pd nanoparticles and the active surface area of metallic Pd was obtained from the specific interaction of a probe molecule with Pd (the CO molecule is a very often used probe molecule for estimation/titration of the metallic surface of palladium[19]). The CO (purity 99.9999%) adsorption isotherm on **Pd@CN-COF** was measured at 273 K on a sample degassed by the same method as for the N_2 adsorption isotherm measurement. The adsorption equilibrium was measured in the range of 0–800 Torr. The adsorption equilibrium threshold was set as a < 0.01 % pressure change on a 20-second interval.

Figure S23 shows the CO adsorption isotherm on the **Pd@CN-COF** catalyst at a temperature of 273 K. The initial, very steep part of the isotherm at the lowest equilibrium pressures clearly indicates a strong interaction of CO molecules with the catalyst. This part of the isotherm is followed by a less steep part of the isotherm representing an adsorption process with a weaker interaction energy. These two processes can be attributed to (a) the interaction of CO with Pd NPs (stronger

[19] G. Agostini, R. Pellegrini, G. Leofanti, L. Bertinetti, S. Bertarione, E. Groppo, A. Zecchina and C. Lamberti, Determination of the Particle Size, Available Surface Area, and Nature of Exposed Sites for Silica-Alumina-Supported Pd Nanoparticles: A Multitechnical Approach, *J. Phys. Chem. C*, 2009, **113**, 10485–10492.

interaction) and (b) the adsorption of CO in the channels of the **CN-COF** support. The quantification of both processes, especially the amount of CO interacting with Pd, was performed by fitting the experimentally measured adsorption isotherm with the sum of two Langmuir adsorption isotherms according to the equation:

$$n_{ads}^{exp} = \frac{n_{max,a} \,.\, b_a \,.\, P}{(1 + b_a \,.\, P)} + \frac{n_{max,b} \,.\, b_b \,.\, P}{(1 + b_b \,.\, P)}$$

where n_{ads}^{exp} is experimentally measured amount adsorbed, b_i is the Langmuir coefficient of the i-th adsorption process, and $n_{max,i}$ is the adsorption capacity (maximum adsorbable amount).

The curves in Figure S23 represent the fit of the data to the dual Langmuir isotherm model. The fit is very good over the entire range of measured data, as is evident from the semi-logarithmic plot. The results of the fit are summarized in Table S3.

Table S3. CO adsorption on **Pd@CN-COF** catalyst: Results of isotherm fit by a sum of two Langmuir isotherm models.

Adsorption process	n_{max} ($cm^3 \cdot g^{-1}$ STP)	b ($Torr^{-1}$)
CO…Pd NPs	1.884	24.11157
CO…CN-COF	2.952	0.00386

The amount of CO molecules, which can be adsorbed on Pd NPs, can be used for the calculation of the number of surface Pd atoms. The main assumption that must be chosen in the calculations is the stoichiometry of CO adsorption on Pd. CO can form linear adsorption complexes (CO...Pd with CO/Pd stoichiometry 1:1) or bridged carbonyls (with CO/Pd stoichiometry 1:2). Usually, a mixture of both types of complexes is formed on the surface (as can be evidenced by C–O vibrational bands in FT-IR spectra, see for example,[19,20] so the average stoichiometry is between 1 and 2. The exact determination of the ratio of linear and bridged carbonyls is difficult. Therefore, in this study, we proceeded to calculate the dispersion, active area of Pd NPs and average size of NPs (see Table S4) assuming both limiting cases, i.e. with the assumption of stoichiometry 1:1 and 1:2. To calculate the active area of Pd NPs, we considered the surface density of Pd atoms 13.21 atoms per 1 nm^2 (based on Pd(100) faces), and for the particle size, the model of spherical nanoparticles

[20] K. I. Hadjiivanov and G. N. Vayssilov, Characterization of oxide surfaces and zeolites by carbon monoxide as an IR probe molecule, *Adv. Catal.*, 2002, **47**, 307–511.

($S_{Pd} = \frac{3}{\varrho_{Pd}\, r_{Pd\,NP}}$). The obtained NP size values (3.2–6.4 nm in diameter) correspond very well with the values determined from XRD using the Scherrer equation (~3.7 nm) and from the analysis of SEM images (5.66 ± 1.27 nm).

Table S4. Assessment of dispersion, specific surface area, and size of Pd nanoparticles of **Pd@CN-COF** catalyst from CO chemisorption.

Stoichiometry	**Surface N_{Pd}** (at·g^{-1})	**Dispersion** (%)	**$S_{Pd,1}$** (m^2·g$_{cat}^{-1}$)	**$S_{Pd,2}$** (m^2·g$_{Pd}^{-1}$)	***d*** (nm)
1:1	$5.054 \cdot 10^{19}$	18.2	3.83	77.9	6.4
1:2	$1.011 \cdot 10^{20}$	36.4	7.65	155.8	3.2

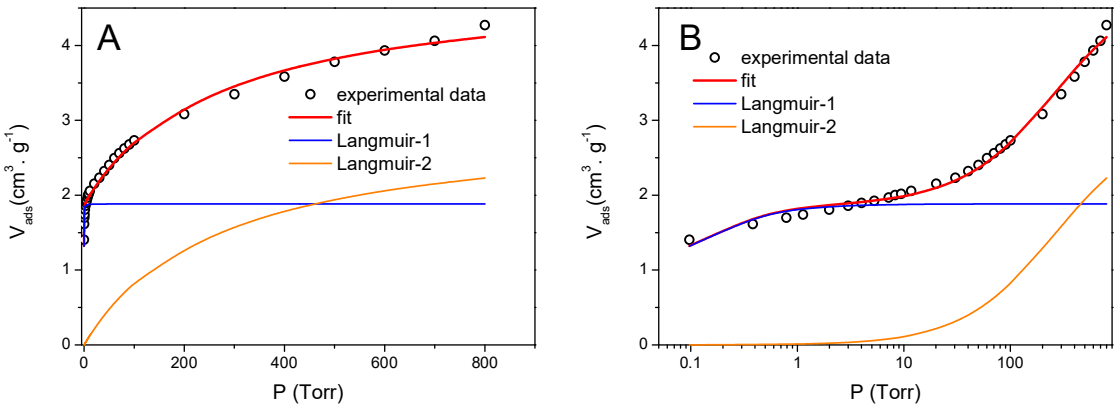

Figure S23. CO adsorption on **Pd@CN-COF** at 273K in linear (A) and semi-logarithmic scale (B).

12. Catalysis with Pd@CN-COF

Starting materials, as well as reagents and solvents, were purchased from TCI, Sigma-Aldrich, MP OrganiX, Fluka, or Penta, and were used as obtained without further purification. 1-Methyl-2-vinylimidazole-4,5-dicarbonitrile and 3-iodoimidazo[1,2-*b*]pyridazine were synthesized according to the literature.[21,22] The solvents were evaporated on a Heidolph Laborota 4001. All reactions were carried out in a Schlenk flask under an inert atmosphere of argon. Column chromatography was performed on silica gel (SiO_2 60, particle size 0.040–0.063 mm, Merck) using commercially available solvents. Thin-layer chromatography was performed on aluminum plates coated with SiO_2 60 F254 silica gel (Merck) and visualized under UV lamp (254 or 365 nm). Melting points were determined in open capillaries on a Büchi B-540 instrument. The mass spectra were measured on a GC/EI-MS configuration consisting of an Agilent 7890B Series GC Custom gas chromatograph. The ^{1}H and ^{13}C NMR spectra were measured in $CDCl_3$ or DMSO-d_6 at 25 °C on a Bruker Ascend™ instrument at 500/125 MHz equipped with a nitrogen-cooled cryoprobe. The chemical shifts are given in ppm relative to the Me_4Si signal. The residual solvent signal was used as an internal standard ($CDCl_3$: 7.24 and 77.23 ppm, DMSO-d_6: 2.50 and 39.51 ppm for ^{1}H and ^{13}C NMR spectra, respectively). The observed signals are described as *s* (singlet), *d* (doublet), *t* (triplet), and *m* (multiplet). Interaction constants (*J*) are given in Hz.

[21] D. M. Johnson and P. G. Rasmussen, An Improved Synthesis of 2-Vinyl-4,5-dicyanoimidazole and Characterization of Its Polymers, *Macromolecules*, 2000, **33**, 8597–8603.
[22] B. Jin, F. Gallou, J. Reilly and B. H. Lipshutz, ppm Pd-catalyzed, Cu-free Sonogashira couplings in water using commercially available catalyst precursors, *Chem. Sci.*, 2019, **10**, 3481–3485.

12.1. Suzuki-Miyaura Reaction

The procedure was modified from the original protocol.[8] Bromobenzene **1** (31.4 mg, 0.2 mmol) or iodobenzene **2** (40.8 mg, 0.2 mmol) and 4-methylphenylboronic acid **3** (27.2 mg, 0.2 mmol) were dissolved in a mixture of DMF/H_2O 1:2 (3 mL), argon was bubbled through the solution for 5 min, whereupon [$Pd(PPh_3)_4$] (1.16 mg, 0.001 mmol, 0.5 mol%) or **Pd@CN-COF** (2 mg, 0.5 mol% Pd), and K_2CO_3 (41.5 mg, 0.3 mmol) were added. PPh_3 (0.52 mg, 0.002 mmol) was eventually added according to the conditions shown in Table S5. The reaction was stirred under argon at 25 °C and was monitored by GC/MS.

Table S5. The Suzuki-Miyaura reaction.

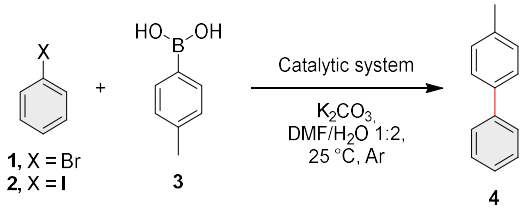

X	Pd catalyst	Catalysis (mol%)	PPh_3	*t* (h)	Conversion (%)[a]	TON	TOF (h^{-1})
Br	[$Pd(PPh_3)_4$]	0.5	×	3	95	190	63.3
Br	**Pd@CN-COF**	0.5	×	0.5	> 99	198	396.0
Br	**Pd@CN-COF**	0.5	✓	1	96	192	192.0
I	[$Pd(PPh_3)_4$]	0.5	×	24	2	4	0.2
I	**Pd@CN-COF**	0.5	×	0.5	97	194	388.0
I	**Pd@CN-COF**	0.5	✓	24	78	156	6.5

[a]Determined by GC/MS.

Table S6. Catalytic performance of known Pd(0)@COF catalysts in the Suzuki-Miyaura reaction.

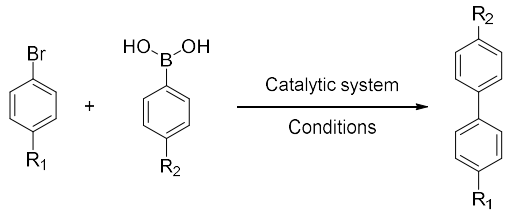

Pd Catalyst	Linkage	R_1, R_2	Catalysis	Solvent system	Base	*T* (°C)	*t* (h)	Conversion/ yield (%)	Ref.
Pd^0/TAT-DHBD	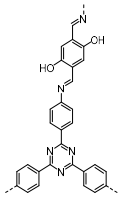	R_1 = Me, R_2 = H	10 mg	DMF	K_2CO_3	100	24	49	23

[23] D. Kaleeswaran, R. Antony, A. Sharma, A. Malani and R. Murugavel, Catalysis and CO_2 Capture by Palladium-Incorporated Covalent Organic Frameworks, *ChemPlusChem*, 2017, **82**, 1253–1265.

Pd^0/TAT-TFP	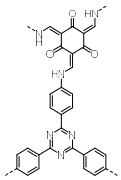	R_1 = Me, R_2 = H	10 mg	DMF	K_2CO_3	100	24	69	23
PdNPs@COF	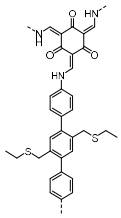	R_1 = Me, R_2 = H	0.1 mol%	DMF/H_2O 1:1	K_2CO_3	50	3	85.7	24
Pd@COF-QA	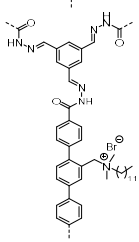	R_1 = H, R_2 = H	1.7 mol%	H_2O	TEA	50	6	99	25
TAPB-BTCA *in situ*	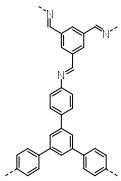	R_1 = H, R_2 = H	0.5 mol%	THF	K_2CO_3 aq.	80	2	51	26
PdNPs@Phos-COF-1	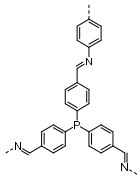	R_1 = Me, R_2 = H	0.35 mol%	DMF/H_2O 1:1	K_2CO_3	50	2	> 99	27
Pd_7/cyano-COF-1	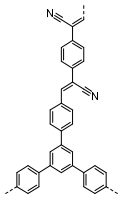	R_1 = Me, R_2 = H	0.3 mol%	DMF/H_2O 1:2	K_2CO_3	25	1	> 99	8
Pd@CN-COF	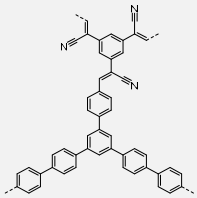	R_1 = H, R_2 = Me	0.5 mol%	DMF/H_2O 1:2	K_2CO_3	25	0.5	> 99	This work

[24] S. Lu, Y. Hu, S. Wan, R. McCaffrey, Y. Jin, H. Gu and W. Zhang, Synthesis of Ultrafine and Highly Dispersed Metal Nanoparticles Confined in a Thioether-Containing Covalent Organic Framework and Their Catalytic Applications, *J. Am. Chem. Soc.*, 2017, **139**, 17082–17088.

[25] J.-C. Wang, C.-X. Liu, X. Kan, X.-W. Wu, J.-L. Kan and Y.-B. Dong, Pd@COF-QA: a phase transfer composite catalyst for aqueous Suzuki–Miyaura coupling reaction, *Green Chem.*, 2020, **22**, 1150–1155.

[26] I. Romero-Muñiz, A. Mavrandonakis, P. Albacete, A. Vega, V. Briois, F. Zamora and A. E. Platero-Prats, Unveiling the Local Structure of Palladium Loaded into Imine-Linked Layered Covalent Organic Frameworks for Cross-Coupling Catalysis, *Angew. Chem. Int. Ed.*, 2020, **59**, 13013–13020.

[27] R. Tao, X. Shen, Y. Hu, K. Kang, Y. Zheng, S. Luo, S. Yang, W. Li, S. Lu, Y. Jin, L. Qui and Q. Zhang, Phosphine-Based Covalent Organic Framework for the Controlled Synthesis of Broad-Scope Ultrafine Nanoparticles, *Small*, 2020, **16**, 1906005.

12.2. Mizoroki-Heck Reaction

The procedure was modified from the original protocol.[8] Bromobenzene **1** (31.4 mg, 0.2 mmol) or iodobenzene **2** (40.8 mg, 0.2 mmol), styrene **5** (20.8 mg, 0.2 mmol), and K_2CO_3 (41.5 mg, 0.3 mmol) were dissolved in NMP (3 mL), argon was bubbled through the solution for 5 min, whereupon [$Pd(PPh_3)_4$] (1.16 mg, 0.001 mmol, 0.5 mol% or 4.62 mg, 0.004 mmol, 2 mol%) or **Pd@CN-COF** (2 mg, 0.5 mol% Pd or 8 mg, 2 mol% Pd) were added. PPh_3 (0.52 mg, 0.002 mmol) was eventually added according to the conditions shown in Table S7. The reaction was stirred under argon at 120 °C and was monitored by GC/MS.

Table S7. The Mizoroki-Heck reaction.

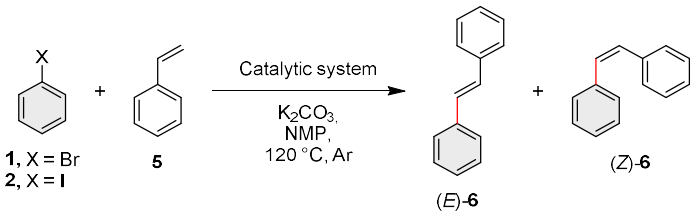

X	Pd catalyst	Catalysis (mol%)	PPh_3	*t* (h)	Conversion (%)[a]	TON	TOF (h^{-1})	Selectivity (%)
Br	[$Pd(PPh_3)_4$]	0.5	×	4	92 (*E*) + 5 (*Z*)	194	48.5	94.8
Br	**Pd@CN-COF**	0.5	×	24	51 (*E*) + 2 (*Z*)	106	4.4	96.2
Br	**Pd@CN-COF**	0.5	✓	24	64 (*E*) + 3 (*Z*)	134	5.6	95.5
Br	[$Pd(PPh_3)_4$]	2	×	3	91 (*E*) + 4 (*Z*)	47.5	15.8	95.8
Br	**Pd@CN-COF**	2	×	24	73 (*E*) + 5 (*Z*)	39	1.6	93.6
Br	**Pd@CN-COF**	2	✓	24	70 (*E*) + 5 (*Z*)	37.5	1.6	93.3
I	[$Pd(PPh_3)_4$]	0.5	×	3	88 (*E*) + 8 (*Z*)	192	64.0	91.7
I	**Pd@CN-COF**	0.5	×	4	88 (*E*) + 8 (*Z*)	192	48.0	91.7
I	**Pd@CN-COF**	0.5	✓	3	89 (*E*) + 8 (*Z*)	194	64.7	91.8

[a]Determined by GC/MS.

12.3. Sonogashira Reaction

The procedure was modified from the original protocol.[28] Bromobenzene **1** (31.4 mg, 0.2 mmol) or iodobenzene **2** (40.8 mg, 0.2 mmol), phenylacetylene **7** (20.4 mg, 0.2 mmol), and DIPA (30.4 mg, 0.3 mmol) were dissolved in anhydrous ACN (3 mL), argon was bubbled through the solution for 5 min, whereupon [$Pd(PPh_3)_4$] (1.16 mg, 0.001 mmol, 0.5 mol%) or **Pd@CN-COF** (2 mg, 0.5 mol% Pd), and CuI (3.81 mg, 0.02 mmol) were added. PPh_3 (0.52 mg, 0.002 mmol) was eventually added according to the conditions shown in Table S8. The reaction was stirred under argon at 80 °C and monitored by GC/MS.

[28] R. S. B. Gonçalves, A. B. V. de Oliveira, H. C. Sindra, B. S. Archanjo, M. E. Mendoza, L. S. A. Carneiro, C. D. Buarque and P. M. Esteves, Heterogeneous Catalysis by Covalent Organic Frameworks (COF): $Pd(OAc)_2$@COF-300 in Cross-Coupling Reactions, *ChemCatChem*, 2016, **8**, 743–750.

Table S8. The Sonogashira reaction.

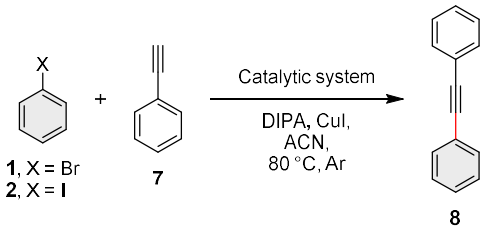

X	Pd catalyst	Catalysis (mol%)	PPh_3	*t* (h)	Conversion (%)[a]	TON	TOF (h^{-1})
Br	$[Pd(PPh_3)_4]$	0.5	×	24	0	0	0
Br	**Pd@CN-COF**	0.5	×	24	0	0	0
Br	**Pd@CN-COF**	0.5	✓	24	0	0	0
I	$[Pd(PPh_3)_4]$	0.5	×	2.5	95	190	76
I	**Pd@CN-COF**	0.5	×	24	72	144	6
I	**Pd@CN-COF**	0.5	✓	2.5	97	194	77.6

[a]Determined by GC/MS.

12.4. Stille Reaction

Bromobenzene **1** (31.4 mg, 0.2 mmol) or iodobenzene **2** (40.8 mg, 0.2 mmol) and 2-(tributylstannyl)thiophene **9** (74.6 mg, 0.2 mmol) were dissolved in anhydrous DMF (3 mL), argon was bubbled through the solution for 5 min, whereupon $[Pd(PPh_3)_4]$ (1.16 mg, 0.001 mmol, 0.5 mol% or 4.62 mg, 0.004 mmol, 2 mol%) or **Pd@CN-COF** (2 mg, 0.5 mol% Pd or 8 mg, 2 mol% Pd) were added. PPh_3 (0.52 mg, 0.002 mmol or 2.10 mg, 0.008 mmol) was eventually added according to the conditions shown in Table S9. The reaction was stirred under argon at 80 or 120 °C and monitored by GC/MS.

Table S9. The Stille reaction.

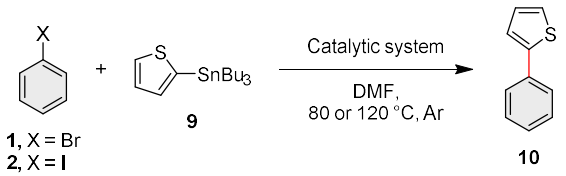

X	Pd catalyst	*T* (°C)	Catalysis (mol%)	PPh_3	*t* (h)	Conversion (%)[a]	TON	TOF (h^{-1})
Br	$[Pd(PPh_3)_4]$	80	0.5	×	5	97	194	38.8
Br	**Pd@CN-COF**	80	0.5	×	24	0	0	0.0
Br	**Pd@CN-COF**	80	0.5	✓	24	42	84	3.5
Br	$[Pd(PPh_3)_4]$	120	0.5	×	2	95	190	95.0
Br	**Pd@CN-COF**	120	0.5	×	24	0	0	0.0
Br	**Pd@CN-COF**	120	0.5	✓	24	74	148	6.2
Br	$[Pd(PPh_3)_4]$	80	2	×	2	95	47.5	23.8
Br	**Pd@CN-COF**	80	2	×	24	0	0	0.0
Br	**Pd@CN-COF**	80	2	✓	24	86	43	1.8
I	$[Pd(PPh_3)_4]$	80	0.5	×	4	95	190	47.5
I	**Pd@CN-COF**	80	0.5	×	24	50	100	4.2
I	**Pd@CN-COF**	80	0.5	✓	4	95	190	47.5

[a]Determined by GC/MS.

12.5. Negishi Reaction

The procedure was modified from the original protocol.[29] *n*-Butyllithium (0.8 mL, 2 mmol, 2.5 M in hexane) was added dropwise to a solution of thiophene (177 mg, 2.1 mmol) in dry THF (10 mL) under argon at 0 °C. Upon completion of the addition, the solution was allowed to warm to 25 °C and stirred for 2 h, whereupon the resulting solution was added to $ZnBr_2$ (495 mg, 2.2 mmol) in dry THF (10 mL). The resulting reaction mixture was stirred at 25 °C for 1 h and the concentration of **11** was determined by titration with iodine in the presence of LiCl.[30]

2-Thienylzinc bromide **11** (2 mL, 0.2 mmol, 0.1 M in THF) was added to a solution of bromobenzene **1** (31.4 mg, 0.2 mmol) or iodobenzene **2** (40.8 mg, 0.2 mmol) in NMP under argon at 25 °C, whereupon $[Pd(PPh_3)_4]$ (1.16 mg, 0.001 mmol, 0.5 mol) or **Pd@CN-COF** (2 mg, 0.5 mol% Pd) were added. PPh_3 (0.52 mg, 0.002 mmol) was eventually added according to the conditions shown in Table S10. The reaction was stirred under argon at 70 °C and monitored by GC/MS.

Table S10. The Negishi reaction.

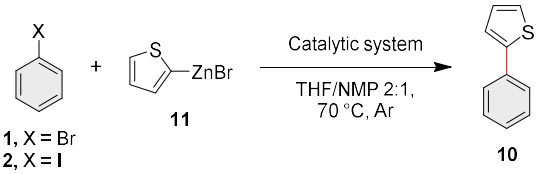

X	Pd catalyst	Catalysis (mol%)	PPh_3	*t* (h)	Conversion (%)[a]	TON	TOF (h^{-1})
Br	$[Pd(PPh_3)_4]$	0.5	×	24	61	122	5.1
Br	**Pd@CN-COF**	0.5	×	24	60	120	5.0
Br	**Pd@CN-COF**	0.5	✓	24	51	102	4.3
I	$[Pd(PPh_3)_4]$	0.5	×	24	90	180	7.5
I	**Pd@CN-COF**	0.5	×	24	87	174	7.3
I	**Pd@CN-COF**	0.5	✓	24	85	170	7.1

[a]Determined by GC/MS.

12.6. Cyanation Reaction

Bromobenzene **1** (31.4 mg, 0.2 mmol) or iodobenzene **2** (40.8 mg, 0.2 mmol), $K_4[Fe)CN)_6]\cdot 3H_2O$ **12** (21.1 mg, 0.05 mmol), and K_2CO_3 (6.91 mg, 0.05 mmol) were dissolved in a mixture of ACN/H_2O 1:1 (3 mL), argon was bubbled through the solution for 5 min, whereupon $[Pd(PPh_3)_4]$ (1.16 mg, 0.001 mmol, 0.5 mol%) or **Pd@CN-COF** (2 mg, 0.5 mol% Pd) were added. KI (16.6 mg, 0.1 mmol) and PPh_3 (0.52 mg,

[29] A. Pelter, I. Jenkins and D. E. Jones, The preparations and some properties of mixed aryl-thienyl oligomers and polymers, *Tetrahedron*, 1997, **53**, 10357–10400.
[30] A. Krasovskiy and P. Knochel, Convenient Titration Method for Organometallic Zinc, Magnesium, and Lanthanide Reagents, *Synthesis*, 2006, **5**, 890–891.

0.002 mmol) were eventually added according to the conditions shown in Table S11. The reaction was stirred under argon at 80 °C and monitored by GC/MS.

Table S11. The cyanation reaction.

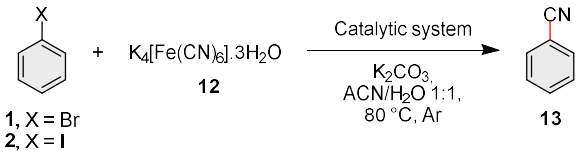

X	Pd catalyst	Catalysis (mol%)	PPh_3	*t* (h)	Conversion (%)[a]	TON	TOF (h^{-1})
Br	$[Pd(PPh_3)_4]$	0.5	×	24	0	0	0
Br	**Pd@CN-COF**	0.5	×	24	0	0	0
Br	**Pd@CN-COF**	0.5	✓	24	0	0	0
Br[b]	$[Pd(PPh_3)_4]$	0.5	×	24	0	0	0
Br[b]	**Pd@CN-COF**	0.5	×	24	0	0	0
Br[b]	**Pd@CN-COF**	0.5	✓	24	0	0	0
I	$[Pd(PPh_3)_4]$	0.5	×	6	> 99	198	33
I	**Pd@CN-COF**	0.5	×	24	0	0	0
I	**Pd@CN-COF**	0.5	✓	10	> 99	198	19.8

[a]Determined by GC/MS. [b]Performed with KI as an additive.

12.7. Allylic Substitution

Allyl acetate **14** (20.0 mg, 0.2 mmol) and diethyl malonate **15** (32.0 mg, 0.2 mmol) were dissolved in absolute EtOH (3 mL), argon was bubbled through the solution for 5 min, whereupon $[Pd(PPh_3)_4]$ (1.16 mg, 0.001 mmol, 0.5 mol%) or **Pd@CN-COF** (2 mg, 0.5 mol% Pd), and EtONa (1 M in EtOH, 0.2 mL, 0.2 mmol) were added. PPh_3 (0.52 mg, 0.002 mmol) was eventually added according to the conditions shown in Table S12. The reaction was stirred under argon at 25 or 50 °C and monitored by GC/MS.

Table S12. The allylic substitution.

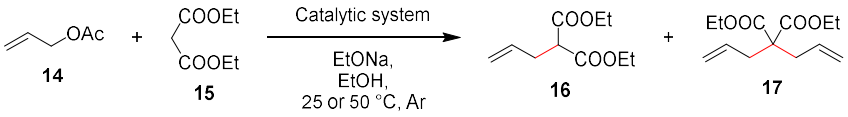

Pd catalyst	*T* (°C)	Catalysis (mol%)	PPh_3	*t* (h)	Conversion to 16/17 (%)[a]	TON	TOF (h^{-1})	Selectivity (%)
$[Pd(PPh_3)_4]$	25	0.5	×	6	70/15	170	28.3	82.4
Pd@CN-COF	25	0.5	×	24	10/-	20	0.8	100.0
Pd@CN-COF	25	0.5	✓	8	72/11	166	20.8	86.7
$[Pd(PPh_3)_4]$	50	0.5	×	0.5	72/14	172	344.0	83.7
Pd@CN-COF	50	0.5	×	24	10/-	20	0.8	100.0
Pd@CN-COF	50	0.5	✓	1	72/14	170	170.0	83.5

[a]Determined by GC/MS.

12.8. Reuse of Pd@CN-COF in the Suzuki-Miyaura Reaction

12.8.1. Recycling Experiments (Catalyst Isolation)

Bromobenzene **1** (942 mg, 6 mmol) and 4-methylphenylboronic acid **3** (816 mg, 6 mmol) were dissolved in a mixture of DMF/H_2O 1:2 (90 mL), argon was bubbled through the solution for 10 min, whereupon **Pd@CN-COF** (60 mg, 0.5 mol% Pd) and K_2CO_3 (1.24 g, 9 mmol) were added. The reaction was stirred under argon at 25 °C for 0.5 h. After the reaction time, **Pd@CN-COF** was separated by a simple filtration, washed with H_2O, EtOH, and DCM, and dried *in vacuo* at 110 °C for 2 hours before use in the subsequent cycle.

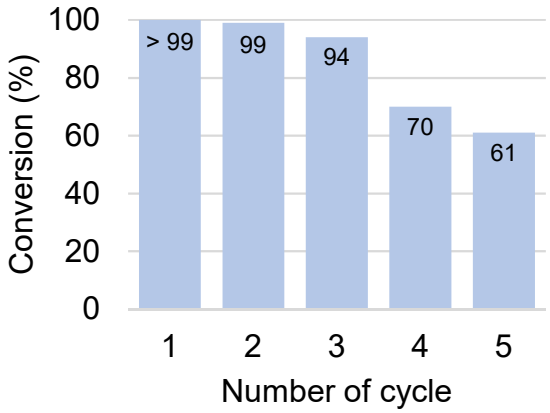

Figure S24. Recycling experiments with **Pd@CN-COF** in the Suzuki-Miyaura reaction. Conversions determined by GC/MS.

12.8.2. Substrate Addition Experiment (No Catalyst Isolation)

Bromobenzene **1** (157 mg, 1 mmol) and 4-methylphenylboronic acid **3** (136 mg, 1 mmol) were dissolved in a mixture of DMF/H_2O 1:2 (15 mL), argon was bubbled through the solution for 10 min, whereupon **Pd@CN-COF** (10 mg, 0.5 mol% Pd) and K_2CO_3 (207 mg, 1.5 mmol) were added. The reaction was stirred under argon at 25 °C for 0.75 h. After this time, another portion of bromobenzene **1** (157 mg, 1 mmol), 4-methylphenylboronic acid **3** (136 mg, 1 mmol), and K_2CO_3 (207 mg, 1.5 mmol) together with additional DMF/H_2O mixture (1:2, 5 mL) was added to the same flask, and the reaction was stirred under argon at 25 °C for another 0.75 h. This procedure was repeated three more times under identical conditions.

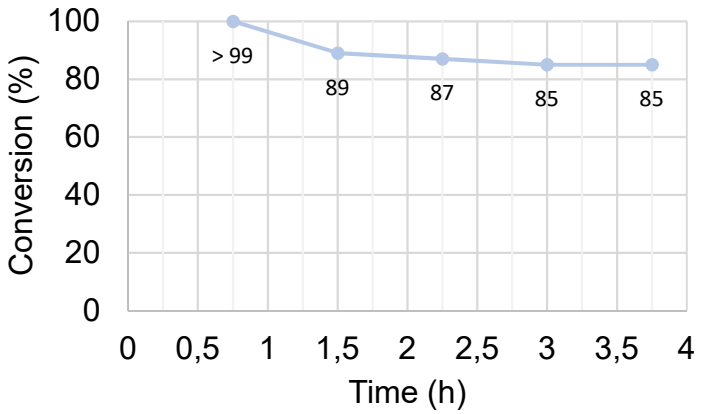

Figure S25. Substrate addition experiment with **Pd@CN-COF** in the Suzuki-Miyaura reaction. Conversions determined by GC/MS.

12.9. Characterization of the Used Pd@CN-COF Catalyst

A used catalyst obtained from the recycling experiments described in Section 12.8.1 was analyzed. The Pd content in **Pd@CN-COF** after five reaction cycles was determined by ICP-MS to be 4.14 wt%.

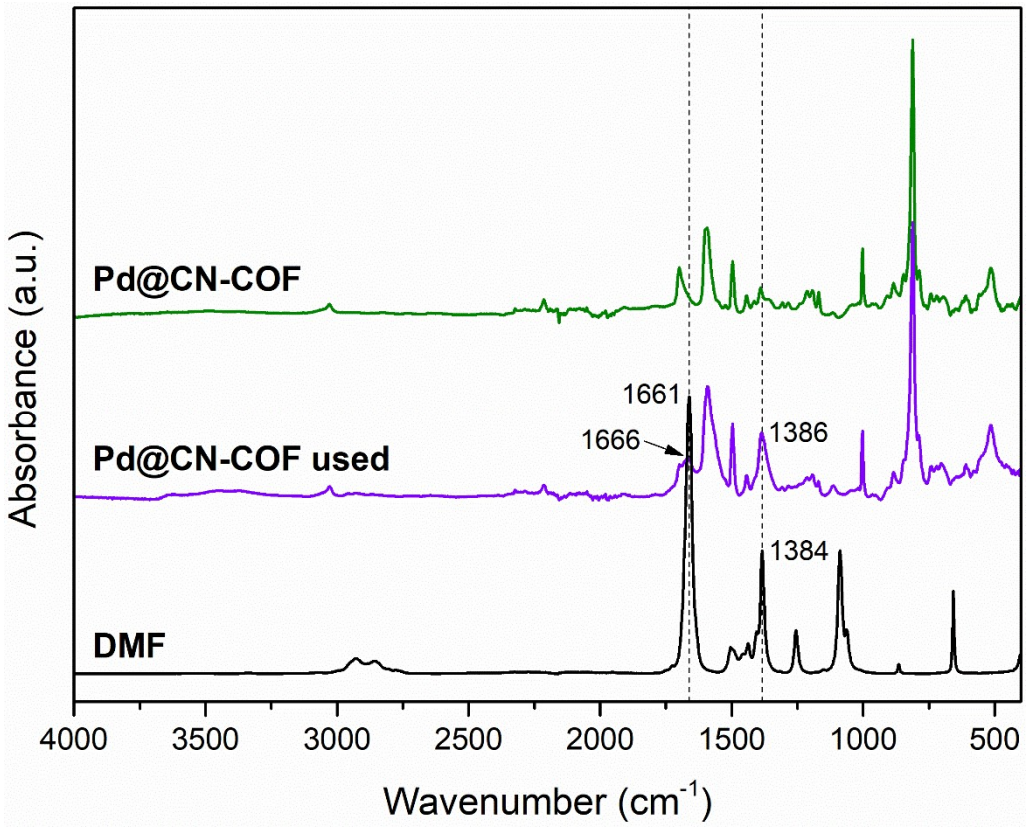

Figure S26. A comparison of FT-IR spectra of **Pd@CN-COF**, used **Pd@CN-COF**, and DMF.

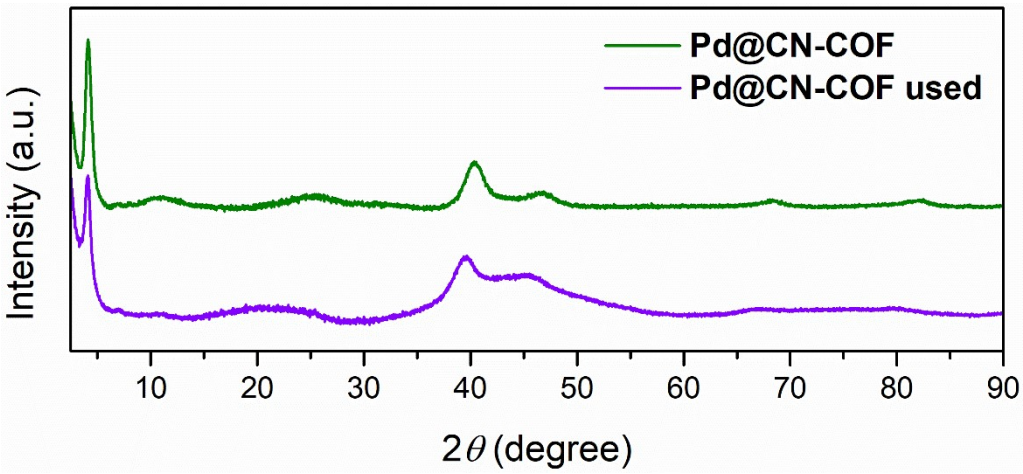

Figure S14. PXRD patterns of **Pd@CN-COF** and used **Pd@CN-COF**.

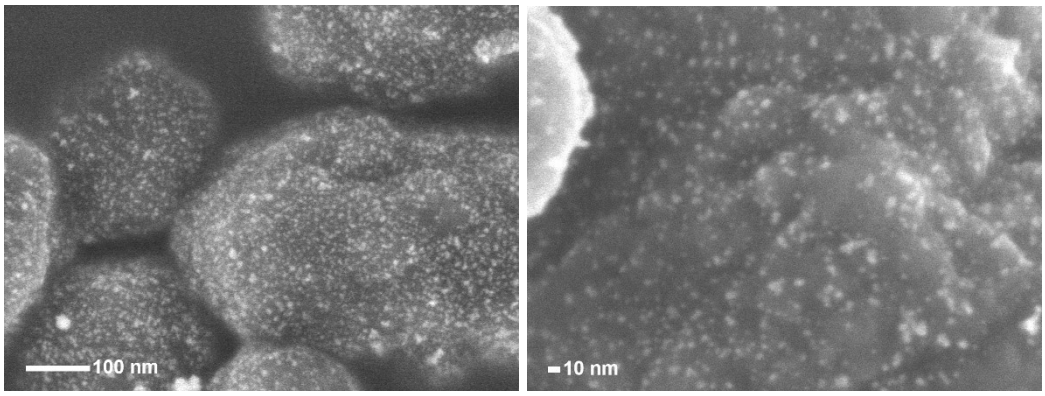

Figure S15. SEM images of used **Pd@CN-COF**.

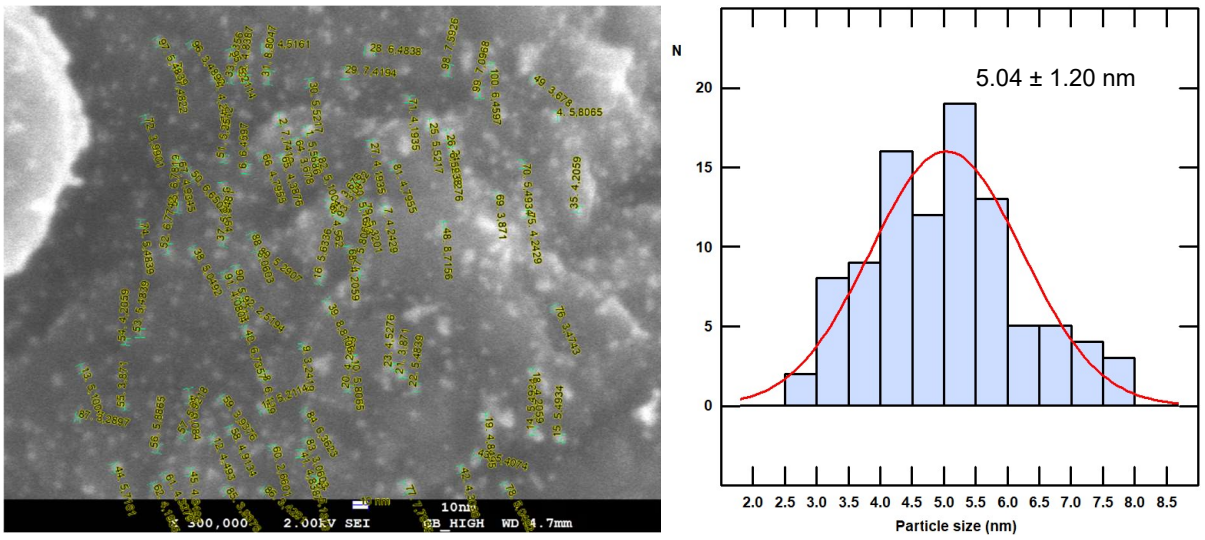

Figure S16. SEM image analysis of used **Pd@CN-COF** (left) with the histogram of particle size distribution (right).

12.9.1. X-ray Photoelectron Spectroscopy

The surface chemical state of the used **Pd@CN-COF** was evaluated and compared with the fresh **Pd@CN-COF**, as shown in Figure S30. The survey spectrum (Figure S30a) of the used catalyst closely resembles that of the fresh one, displaying the same elements. However, the Pd signal intensity is higher, indicating an enrichment of Pd on the catalyst surface after reuse. The C 1s high-resolution spectra (Figure S30b) reveal the same chemical species in both cases, with the additional presence of K^+ in the used catalyst, originating from the base used during the reaction. Another notable difference is the higher concentration of C=O bonds in the used catalyst. Although the corresponding components are not well resolved due to low intensity in the spectra, Table S13 clearly shows the difference in atomic concentrations. The O 1s high-resolution spectra (Figure S30c) exhibit significant overlap between the Pd $3p_{3/2}$ and O 1s signals. Peak fitting identifies two oxygen species: C–O bonds at 532.3 eV[9] and C=O bonds at 531.4 eV.[9] These spectra clearly highlight an increase in C=O species for the used catalyst. Finally, the Pd 3d spectra (Figure S30d) show the same Pd species in both samples, but with a clear reduction of Pd in the used catalyst, where the surface amount of metallic Pd is 11.7 times higher than that of its combined counterparts. Overall, the enrichment of C=O bonds and the reduction of Pd in the used catalyst can be attributed to the effect of DMF during the reactions, which leads to organic deposits and Pd reduction.

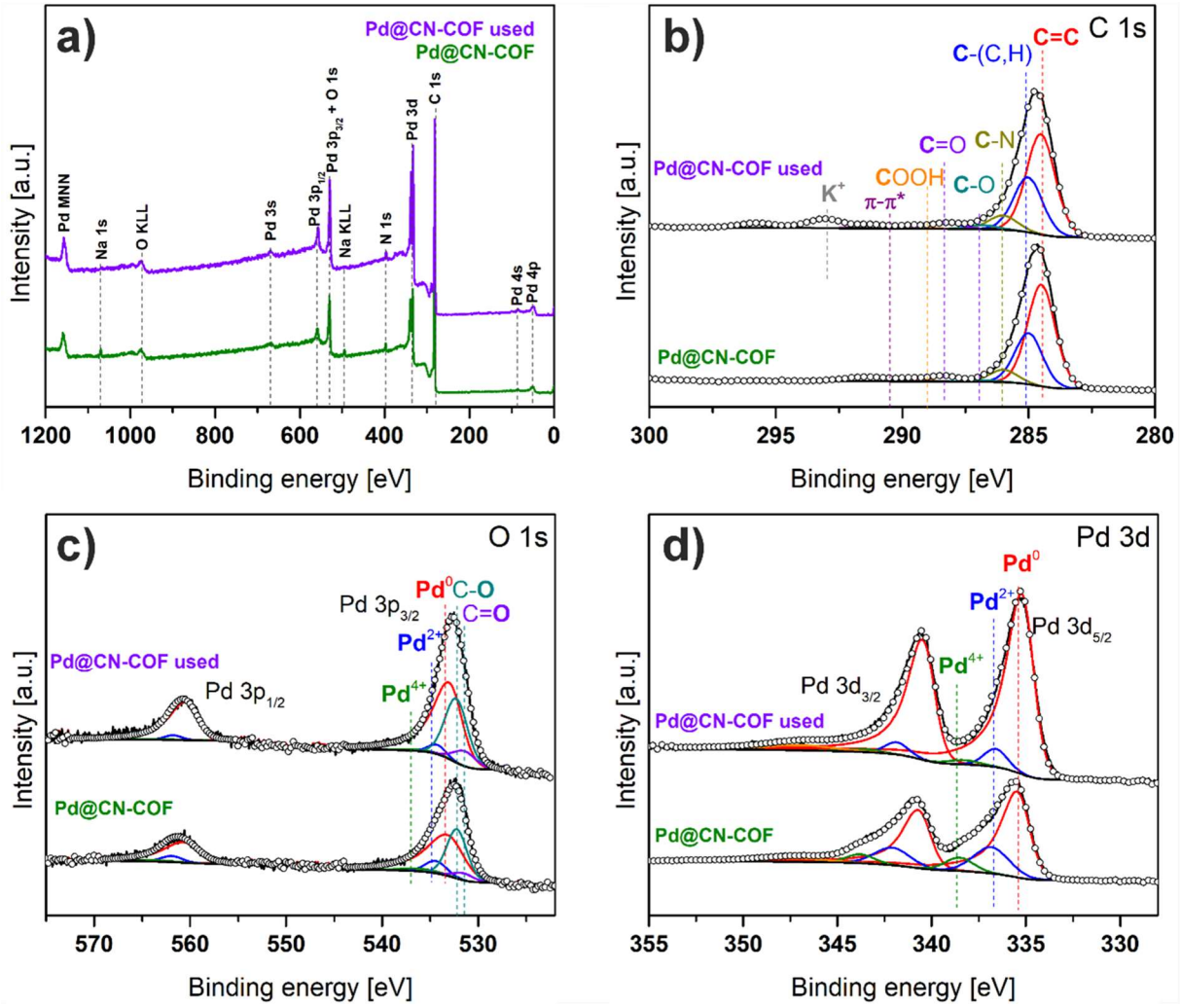

Figure S30. XPS spectra of **Pd@CN-COF** and used **Pd@CN-COF**. The survey spectra (a), high-resolution spectra of C 1s (b), N 1s (c), and Pd 3d (d).

Table S13. Atomic concentration of **Pd@CN-COF** and used **Pd@CN-COF** surface chemical species determined by XPS.

Sample	Atomic concentration [%]													
	Pd^0	**Pd^{2+}**	**Pd^{4+}**	**C=C**	**C–(C,H)**	**C–N**	**C–O**	**C=O**	**COOH**	**K^+**	**C–O**	**C=O**	**C–N**	**Na^+**
Pd@CN-COF	4.32	1.21	0.40	49.73	22.45	5.80	2.09	1.26	1.15	–	6.87	0.99	2.72	1.01
Pd@CN-COF used	7.02	0.45	0.15	39.06	22.73	6.54	2.04	2.24	1.36	1.65	10.85	2.68	2.92	0.31

12.9.2. Volumetry

The textural properties and active surface of Pd nanoparticles in the used catalyst were characterized by N_2 adsorption at 77 K (Figure S31) and CO at 273 K (Figure S32). From the nitrogen adsorption, it is clear that the used catalyst shows a very obvious decrease in the size of the specific surface area and pore volume, although the character of the isotherm (shape) remains preserved and therefore there are no changes in the pore size. The surface area decreased from 358 $m^2 \cdot g^{-1}$ of the fresh catalyst to 204 $m^2 \cdot g^{-1}$, while the total pore volume decreased from the original 0.225 $cm^3 \cdot g^{-1}$ to 0.12 $cm^3 \cdot g^{-1}$.

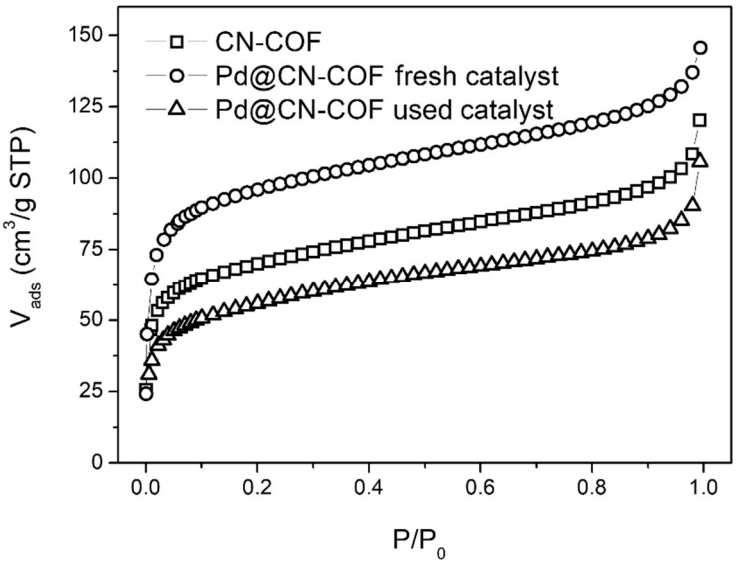

Figure S31. N_2 adsorption isotherm of parent **CN-COF** (squares), fresh **Pd@CN-COF** catalyst (circles), and used **Pd@CN-COF** catalyst (up triangle) at 77 K.

Figure S32 shows the CO adsorption isotherm at 273 K on the used catalyst. Compared to the CO isotherm of the fresh catalyst (cf. Figure S23), a dramatic decrease in the strong interaction of CO with the Pd surface is evident. The fit of the isotherm with the dual Langmuirian adsorption model (see Table S14) shows that the amount of CO interacting with Pd atoms decreased by almost a tenth (from the original 1.884 $cm^3 \cdot g^{-1}$ to 0.234 $cm^3 \cdot g^{-1}$).

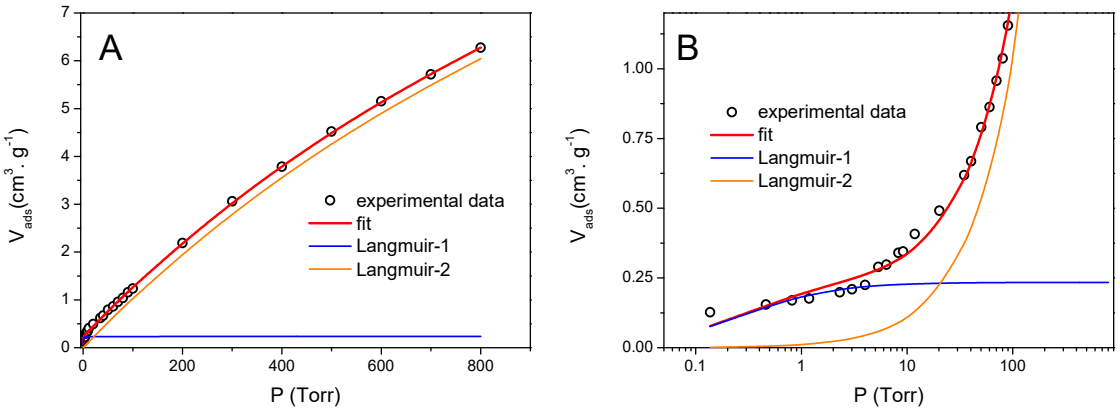

Figure S32. CO adsorption on the used **Pd@CN-COF** at 273K in linear (A) and semi-logarithmic scale (B).

Under the same assumptions as in the case of the evaluation of the CO isotherm of the fresh catalyst, the dispersion of Pd is between 2.69 and 5.37 %. From the geometric model of spherical particles, this would mean an increase in the average size of Pd nanoparticles from 3.2–6.4 nm to 11–21 nm. However, this was not observed in the SEM images, where the Pd nanoparticles on the support surface show almost identical sizes and size distribution as on the fresh catalyst (see Figures S16 and S29). Significant sintering of Pd nanoparticles is not confirmed by PXRD analysis (see Figure S27), which, in agreement with SEM, shows an almost constant size of Pd nanoparticles. We attribute the significant decrease in the amount of CO interacting with Pd atoms to the blocking of the Pd surface by more strongly bound organic molecules originating from the tested reactions, as also indicated by FT-IR spectroscopy of the used catalyst (Figure S26).

Table S14. Assessment of dispersion, specific surface area, and size of Pd nanoparticles of the used **Pd@CN-COF** catalyst from CO chemisorption.

Stoichiometry	**Surface N_{Pd}** ($at \cdot g^{-1}$)	**Dispersion** (%)	**$S_{Pd,1}$** ($m^2 \cdot g_{cat}^{-1}$)	**$S_{Pd,2}$** ($m^2 \cdot g_{Pd}^{-1}$)	***d*** (nm)
1:1	$6.291 \cdot 10^{18}$	2.7	0.48	11.5	21.7
1:2	$1.258 \cdot 10^{19}$	5.4	0.95	23.0	10.8

12.10. Pd@CN-COF Catalysis Towards Valuable Products

12.10.1. Synthesis of 4'-Chloro-2-nitro-1,1'-biphenyl (20)

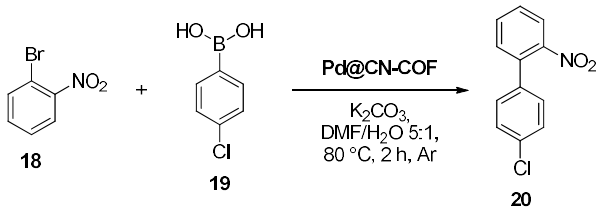

2-Bromonitrobenzene **18** (404 mg, 2 mmol) and 4-chlorophenylboronic acid **19** (313 mg, 2 mmol) were dissolved in a mixture of DMF/H_2O 5:1 (30 mL), argon was bubbled through the solution for 10 min, whereupon **Pd@CN-COF** (20 mg, 0.5 mol%) and K_2CO_3 (415 mg, 3 mmol) were added, and the reaction was stirred under argon at 80 °C for 2 h. **Pd@CN-COF** was separated by filtration and the filtrate was diluted with water and extracted with DCM (3×20 mL). The combined organic extracts were washed with water (3×50 mL), brine (30 mL), dried (Na_2SO_4), and the solvent was evaporated under reduced pressure. The crude product was purified by column chromatography (SiO_2; DCM/Hex 2:3). Yield: 446 mg (96 %). Yellow solid. M. p. = 65–67 °C (lit.[31] 64 °C). R_f = 0.6 (SiO_2; DCM/Hex 2:3). ^{1}H NMR (500 MHz, 25 °C, $CDCl_3$): δ = 7.87–7.85 (m, 1H, Ar), 7.62–7.59 (m, 1H, Ar), 7.50–7.47 (m, 1H, Ar), 7.40–7.37 (m, 3H, Ar), 7.24–7.22 (m, 2, Ar) ppm. ^{13}C NMR (125 MHz, 25 °C, $CDCl_3$): δ = 149.25, 136.09, 135.41, 134.66, 132.69, 132.04, 129.46, 129.12, 128.76, 124.47 ppm. EI-MS (70 eV) *m/z* (rel. in.): 233 ([M]$^+$, 50), 198 (38), 168 (42), 152 (100), 142 (28), 115 (26), 76 (17).

12.10.2. Synthesis of 3-(Benzo[d][1,3]dioxol-5-yl)prop-2-yn-1-ol (23)

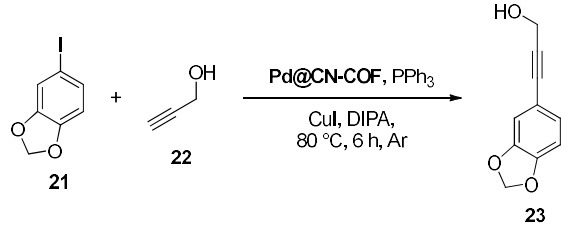

5-Iodobenzo[*d*][1,3]dioxole **21** (496 mg, 2 mmol) and propargyl alcohol **22** (112 mg, 2 mmol) were dissolved in DIPA (20 mL), argon was bubbled through the

[31] F.-X. Felpin, E. Fouquet and C. Zakri, Improved Suzuki–Miyaura Reactions of Aryldiazonium Salts with Boronic Acids by Tuning Palladium on Charcoal Catalyst Properties, *Adv. Synth. Catal.*, 2009, **351**, 649–655.

solution for 10 min, whereupon **Pd@CN-COF** (20 mg, 0.5 mol%), PPh_3 (5.25 mg, 0.02 mmol), and CuI (38.1 mg, 0.2 mmol) were added, and the reaction was stirred under argon at 80 °C for 6 h. The solvent was evaporated under reduced pressure, and the resulting material was dissolved in DCM (20 mL). Saturated aqueous NH_4Cl (20 mL) was added, the organic phase was separated, the aqueous one was extracted with DCM (2×20 mL), the combined organic extracts were dried (Na_2SO_4), and the solvent was evaporated under reduced pressure. The crude product was purified by column chromatography (SiO_2; Hex/EtOAc 1:1). Yield: 314 mg (90 %). Yellowish solid. M. p. = 76–78 °C (lit.[32] 74–76 °C). R_f = 0.7 (SiO_2; Hex/EtOAc 1:1). ^{1}H NMR (500 MHz, 25 °C, $CDCl_3$): δ = 6.95–6.93 (m, 1H, Ar), 6.86–6.85 (m, 1H, Ar), 6.73–6.72 (m, 1H, Ar), 5.95 (s, 2H, CH_2), 4.45 (d, 2H, J = 6.1 Hz, CH_2OH), 1.77 (t, 1H, J = 6.1 Hz, OH) ppm. ^{13}C NMR (125 MHz, 25 °C, $CDCl_3$): δ = 148.25, 147.58, 126.60, 115.90, 111.87, 108.64, 101.53, 85.78, 85.76, 51.86 ppm. EI-MS (70 eV) *m/z* (rel. in.): 176 ([M]$^+$, 100), 159 (19), 147 (38), 118 (17), 89 (29), 63 (13).

12.10.3. Synthesis of 3-(Phenylethynyl)imidazo[1,2-b]pyridazine (25)

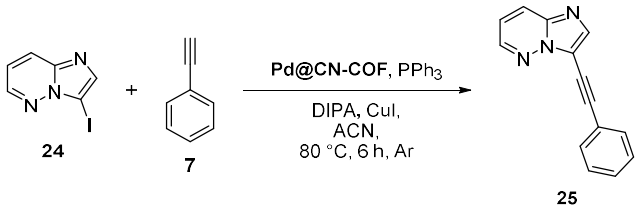

3-Iodoimidazo[1,2-*b*]pyridazine **24** (490 mg, 2 mmol), phenylacetylene **7** (204 mg, 2 mmol), and DIPA (304 mg, 3 mmol) were dissolved in anhydrous ACN (30 mL), argon was bubbled through the solution for 10 min, whereupon **Pd@CN-COF** (20 mg, 0.5 mol%), PPh_3 (5.25 mg, 0.02 mmol), and CuI (38.1 mg, 0.2 mmol) were added, and the reaction was stirred under argon at 80 °C for 6 h. The solvent was evaporated under reduced pressure and the resulting material was dissolved in DCM (20 mL). Saturated aqueous NH_4Cl (20 mL) was added, the organic phase was separated, the aqueous one was extracted with DCM (2×20 mL), the combined organic extracts were dried (Na_2SO_4), and the solvent was evaporated under reduced pressure. The crude product was purified by column chromatography (SiO_2; EtOAc). Yield: 398 mg (91 %). Yellow solid. M. p. = 138–140 °C. R_f = 0.4 (SiO_2; EtOAc).

[32] V. Gudla and R. Balamurugan, Synthesis of Arylnaphthalene Lignan Scaffold by Gold-Catalyzed Intramolecular Sequential Electrophilic Addition and Benzannulation, *J. Org. Chem.*, 2011, **76**, 9919–9933.

^{1}H NMR (500 MHz, 25 °C, $CDCl_3$): δ = 8.45–8.44 (m, 1H, HetAr), 8.03 (s, 1H, HetAr), 7.97–7.95 (m, 1H, HetAr), 7.61–7.59 (m, 2H, Ar), 7.36–7.34 (m, 3H, Ar), 7.10–7.07 (m, 1H, HetAr) ppm. ^{13}C NMR (125 MHz, 25 °C, $CDCl_3$): δ = 144.00, 139.80, 138.62, 131.89, 129.05, 128.58, 126.11, 122.56, 117.70, 113.55, 98.94, 76.03 ppm. EI-MS (70 eV) *m/z* (rel. in.): 219 ([M]$^+$, 100), 164 (5), 126 (5), 114 (17).

12.10.4. Synthesis of 4,7-Di(thiophen-2-yl)benzo[c][1,2,5]thiadiazole (27)

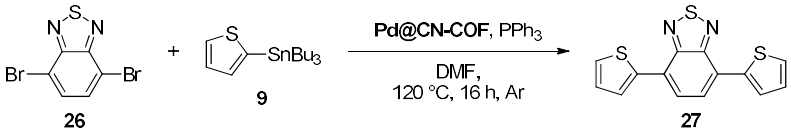

4,7-Dibromobenzo[*c*][1,2,5]thiadiazole **26** (294 mg, 1 mmol) and 2-(tributylstannyl)thiophene **9** (746 mg, 2 mmol) were dissolved in anhydrous DMF (15 mL), argon was bubbled through the solution for 10 min, whereupon **Pd@CN-COF** (20 mg, 1 mol%) and PPh_3 (5.25 mg, 0,02 mmol) were added, and the reaction was stirred under argon at 120 °C for 16 h. The reaction mixture was poured into water (20 mL), and the solid was filtered off. The solid was washed with DCM to remove crude product from the catalyst, and the filtrate was washed with water (3×20 mL), dried (Na_2SO_4), and the solvent was evaporated under reduced pressure. The resulting material was triturated with a minimum amount of hexane, and the solid was separated by filtration. Yield: 267 mg (89 %). Red solid. M. p. = 122–123 °C (lit.[33] 123–124 °C). ^{1}H NMR (500 MHz, 25 °C, $CDCl_3$): δ = 8.10–8.09 (m, 2H, Th), 7.85 (s, 2H, Ar), 7.45–7.44 (m, 2H, Th), 7.20–7.19 (m, 2H, Th) ppm. ^{13}C NMR (125 MHz, 25 °C, $CDCl_3$): δ = 152.85, 139.56, 128.23, 127.71, 127.03, 126.21, 126.00 ppm. EI-MS (70 eV) *m/z* (rel. in.): 300 ([M]$^+$, 100), 207 (11).

[33] H. A. Patel, V. J. Bhanvadia, H. M. Mande, S. S. Zade and A. L. Patel, Benzochalcogendiazole-based conjugated molecules: investigating the effects of substituents and heteroarom juggling, *Org. Biomol. Chem.*, 2019, **17**, 9467–9478.

12.10.5. One-Pot Synthesis of 1-Methyl-2-(4-(thiophen-2-yl)styryl)-1H-imidazole-4,5-dicarbonitrile (32)

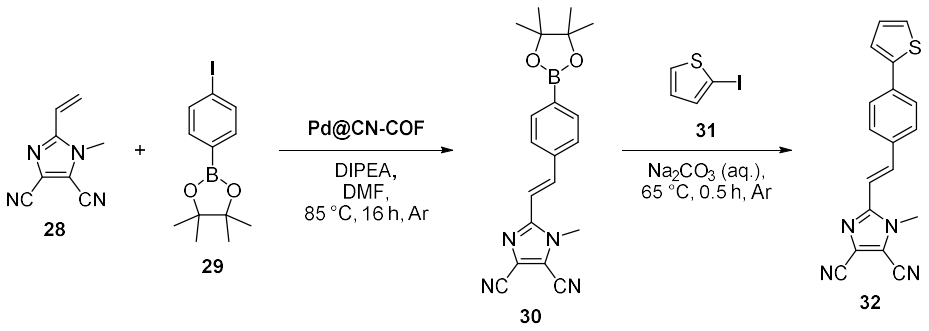

1-Methyl-2-vinylimidazole-4,5-dicarbonitrile **28** (158 mg, 1 mmol), 4-iodophenylboronic acid pinacol ester **29** (330 mg, 1 mmol), and DIPEA (194 mg, 1,5 mmol) were dissolved in anhydrous DMF (15 mL), argon was bubbled through the solution for 10 min, whereupon **Pd@CN-COF** (40 mg, 2 mol% Pd) was added, and the reaction was stirred under argon at 85 °C for 16 h. The reaction temperature was then decreased to 65 °C, whereupon 2-iodothiophene **31** (210 mg, 1 mmol) and Na_2CO_3 (127 mg, 1.2 mmol) in H_2O (3 mL) were added *via* syringe, and the reaction was stirred under argon for another 0.5 h. The reaction mixture was poured into water (20 mL), and the solid was filtered off. The filtered solid was washed with DCM to remove the crude product from the catalyst, and the filtrate was washed with water (3×20 mL), dried (Na_2SO_4), and the solvent was evaporated under reduced pressure. The crude product was purified by column chromatography (SiO_2; DCM). Yield: 104 mg (33 %). Yellow solid. M. p. = 271–274 °C. R_f = 0.7 (SiO_2; DCM). ^{1}H NMR (500 MHz, 25 °C, DMSO-d_6): δ = 7.83–7.81 (m, 2H, Ar), 7.72–7.69 (m, 3H, Ar + CH=), 7.62–7.59 (m, 2H, Th), 7.37–7.33 (m, 1H, CH=), 7.17–7.15 (m, 1H, Th), 3.90 (s, 3H, CH_3) ppm. ^{13}C NMR (125 MHz, 25 °C, DMSO-d_6): δ = 150.58, 142.66, 137.66, 134.79, 134.23, 128.72, 128.68, 126.45, 125.61, 124.53, 120.57, 113.28, 112.66, 11.93, 109.15, 33.04 ppm. EI-MS (70 eV) *m/z* (rel. in.): 315 ([M]$^+$, 100), 300 (15), 207 (8), 158 (5).

12.11. NMR Spectra of Products 20, 23, 25, 27, and 32

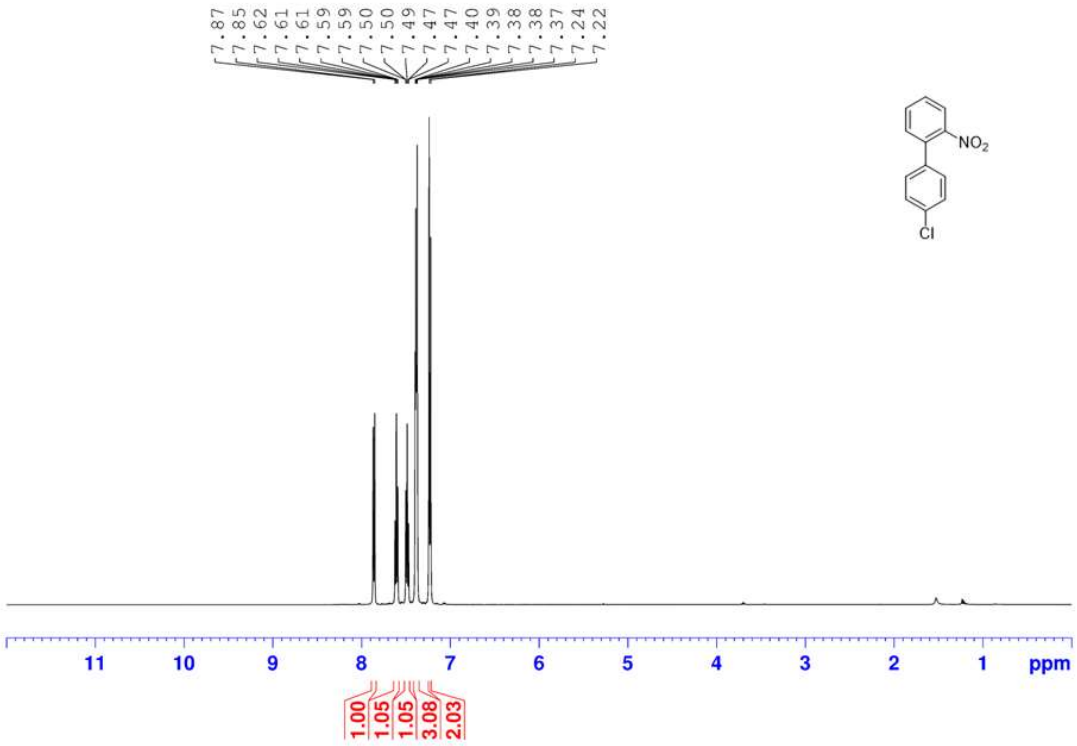

Figure S33. ^{1}H NMR (500 MHz, $CDCl_3$, 25 °C) spectrum of compound **20**.

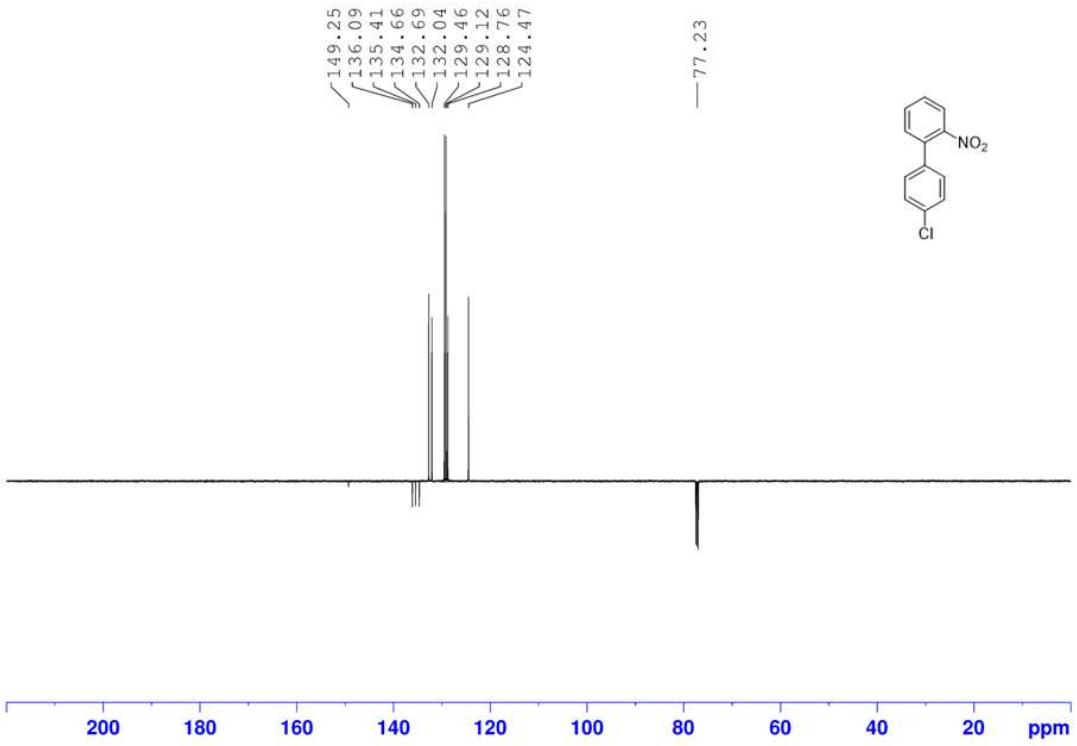

Figure S34. ^{13}C NMR (125 MHz, $CDCl_3$, 25 °C) spectrum of compound **20**.

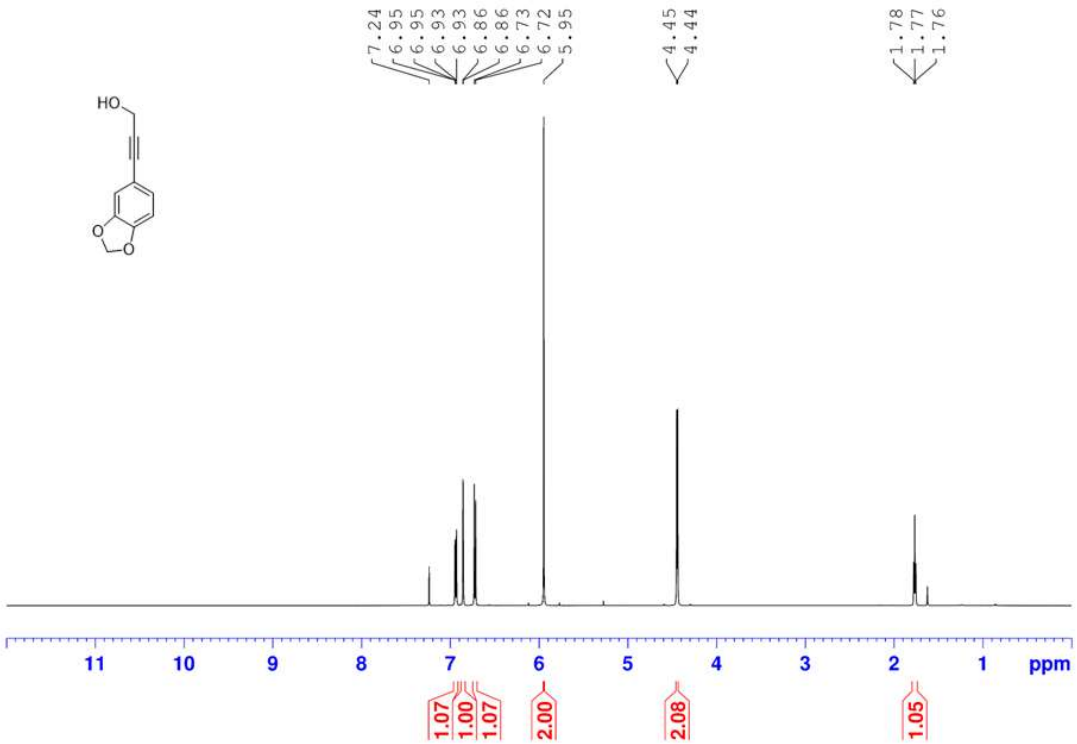

Figure S35. ^{1}H NMR (500 MHz, $CDCl_3$, 25 °C) spectrum of compound **23**.

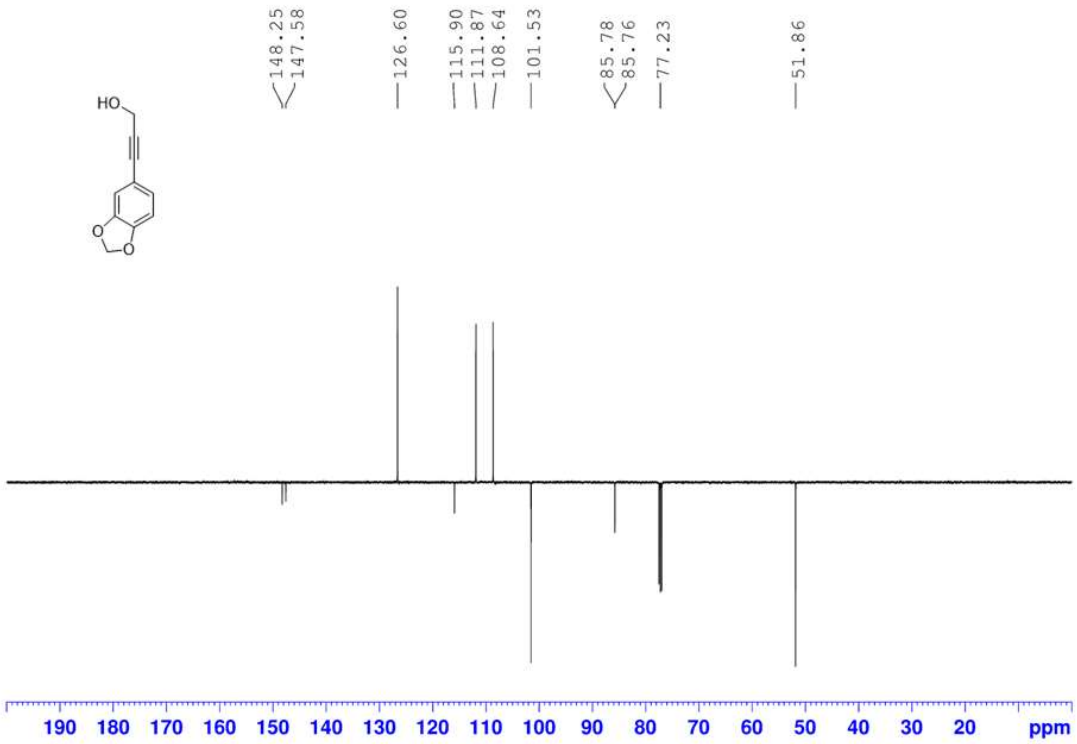

Figure S36. ^{13}C NMR (125 MHz, $CDCl_3$, 25 °C) spectrum of compound **23**.

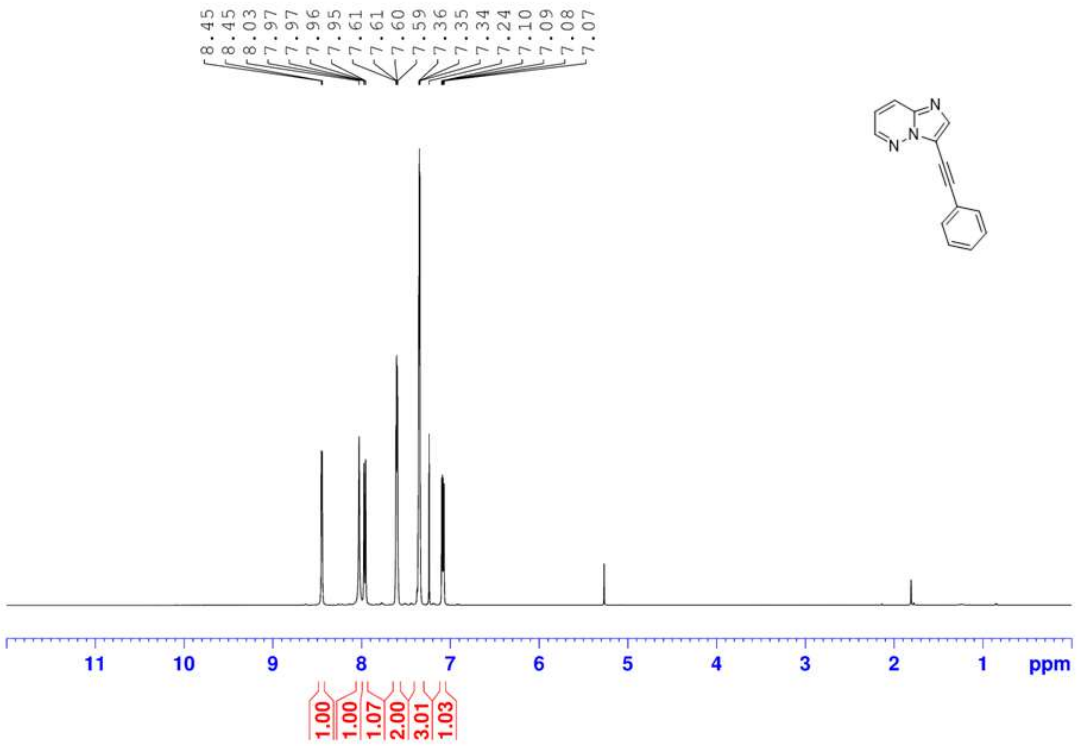

Figure S37. ^{1}H NMR (500 MHz, $CDCl_3$, 25 °C) spectrum of compound **25**.

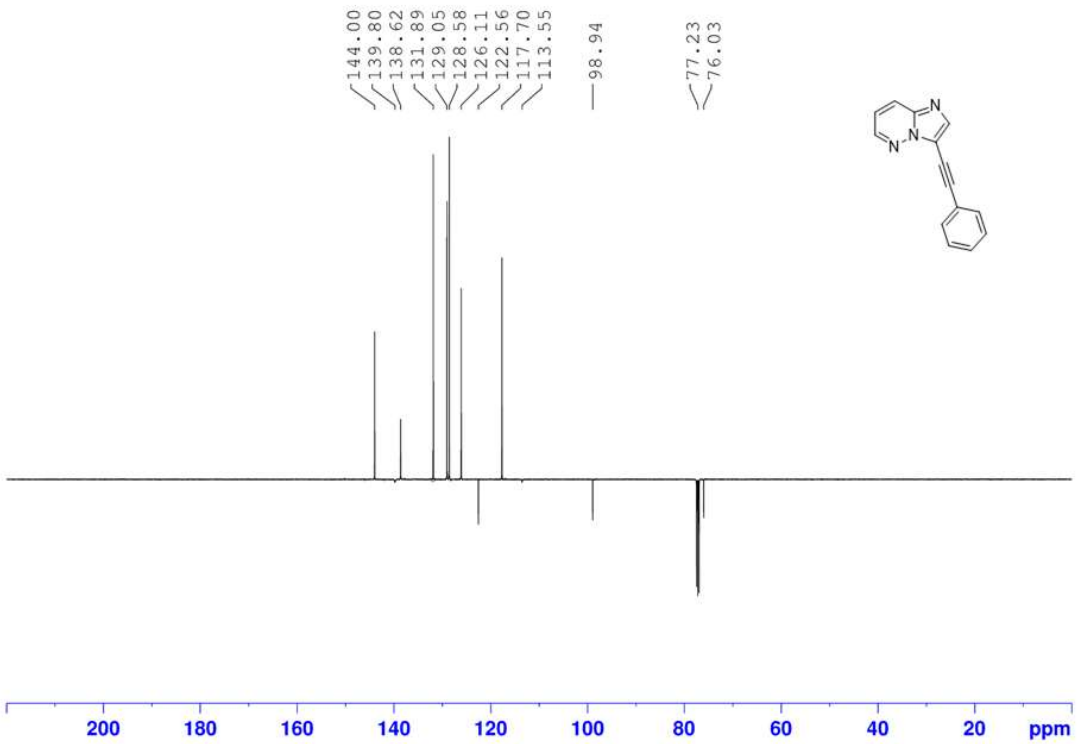

Figure S38. ^{13}C NMR (125 MHz, $CDCl_3$, 25 °C) spectrum of compound **25**.

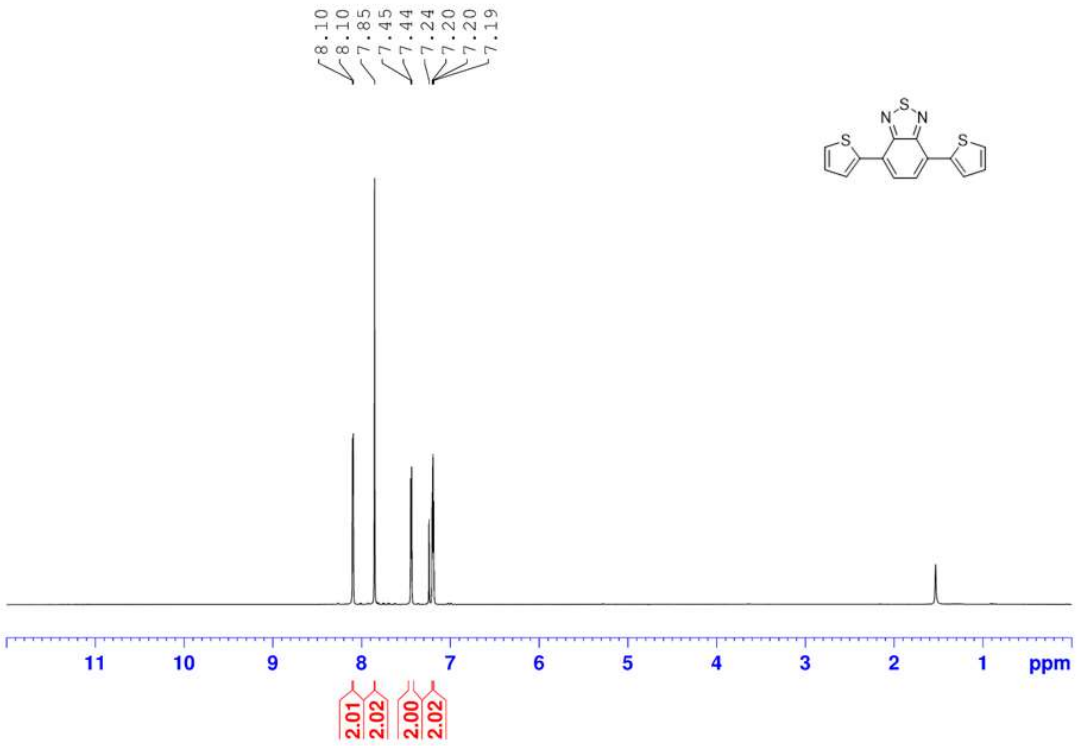

Figure S39. ^{1}H NMR (500 MHz, $CDCl_3$, 25 °C) spectrum of compound **27**.

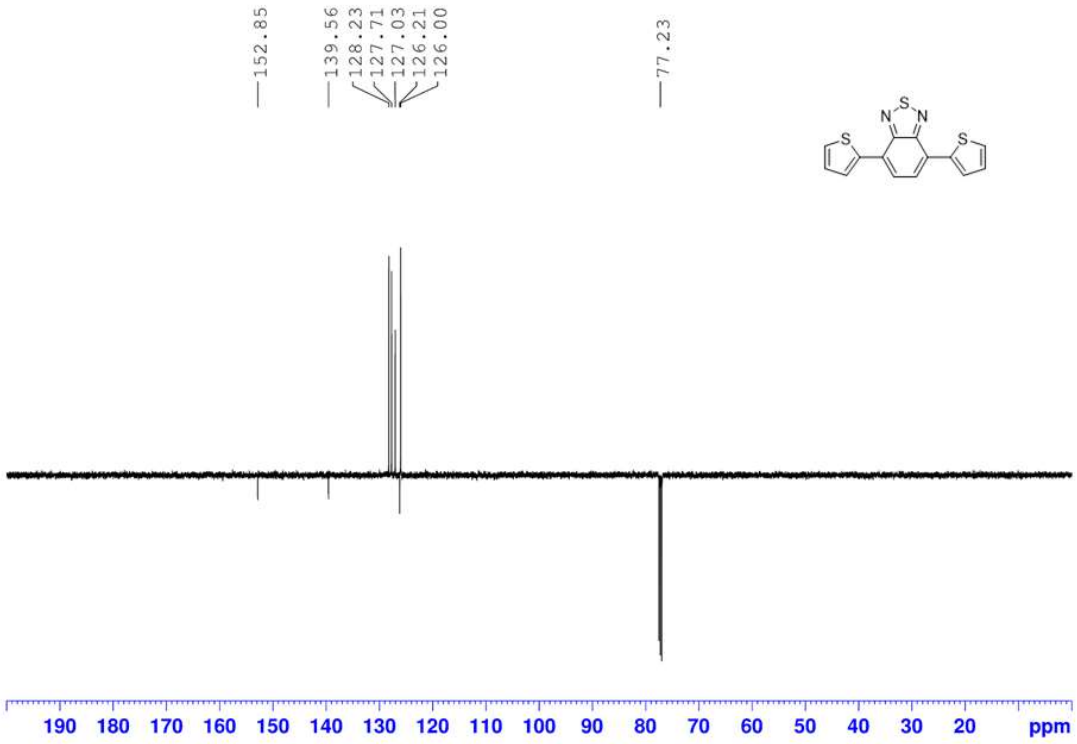

Figure S40. ^{13}C NMR (125 MHz, $CDCl_3$, 25 °C) spectrum of compound **27**.

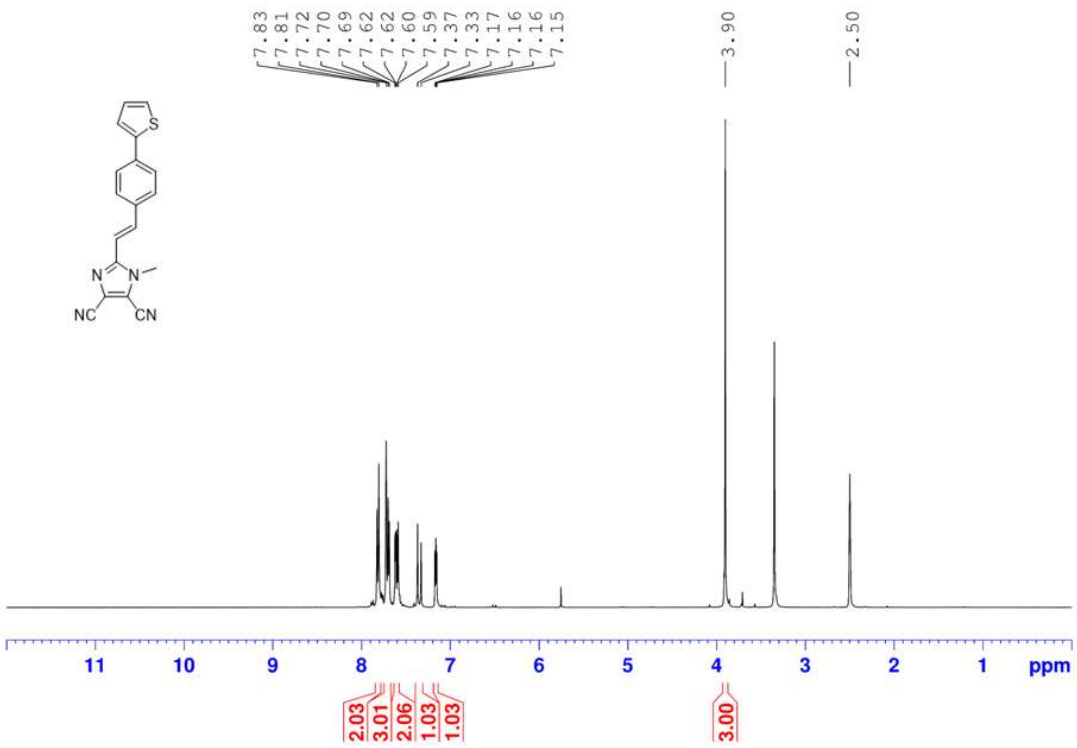

Figure S41. ^{1}H NMR (500 MHz, DMSO-d_6, 25 °C) spectrum of compound **32**.

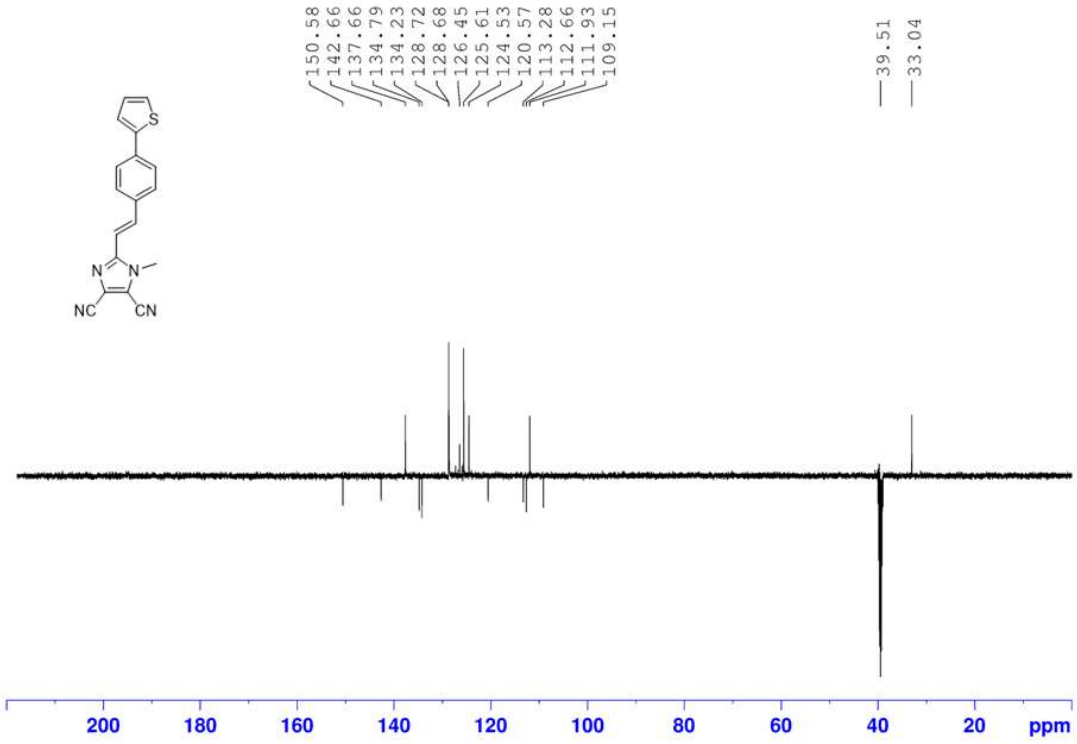

Figure S42. ^{13}C NMR (125 MHz, DMSO-d_6, 25 °C) spectrum of compound **32**.

12.12. Evaluation of the Catalytic Activity

Table S15. Catalytic efficiency of **Pd@CN-COF** vs. $[Pd(PPh_3)_4]$.

					Pd@CN-COF				$[Pd(PPh_3)_4]$			
Reaction	**X**	**Catalysis (mol%)**	***T* (°C)**	**PPh_3**	***t* (h)**	**Conversion (%)**	**TON**	**TOF**	***t* (h)**	**Conversion (%)**	**TON**	**TOF**
Suzuki-Miyaura	Br	0.5	25	×	0.5	99	198	396.0	3	95	190	63.3
	I	0.5	25	×	0.5	97	194	388.0	24	2	4	0.2
Mizoroki-Heck	Br	2	120	×	24	78	39	1.6	3	95	47.5	15.8
	I	0.5	120	×	4	96	192	48.0	3	96	192	64.0
Sonogashira	Br	0.5	80	✓	24	0	0	0.0	24	0	0	0.0
	I	0.5	80	✓	2.5	97	194	77.6	2.5	95	190	76.0
Stille	Br	2	80	✓	24	86	43	1.8	2	95	47.5	23.8
	I	0.5	80	✓	4	95	190	47.5	4	95	190	47.5
Negishi	Br	0.5	65	×	24	60	120	5.0	24	61	122	5.1
	I	0.5	65	×	24	87	174	7.3	24	90	180	7.5
Cyanation	Br	0.5	80	✓	24	0	0	0.0	24	0	0	0.0
	I	0.5	80	✓	10	99	198	19.8	6	99	198	33.0
Allylic substitution	–	0.5	50	✓	1	72	144	144.0	0.5	72	144	288.0

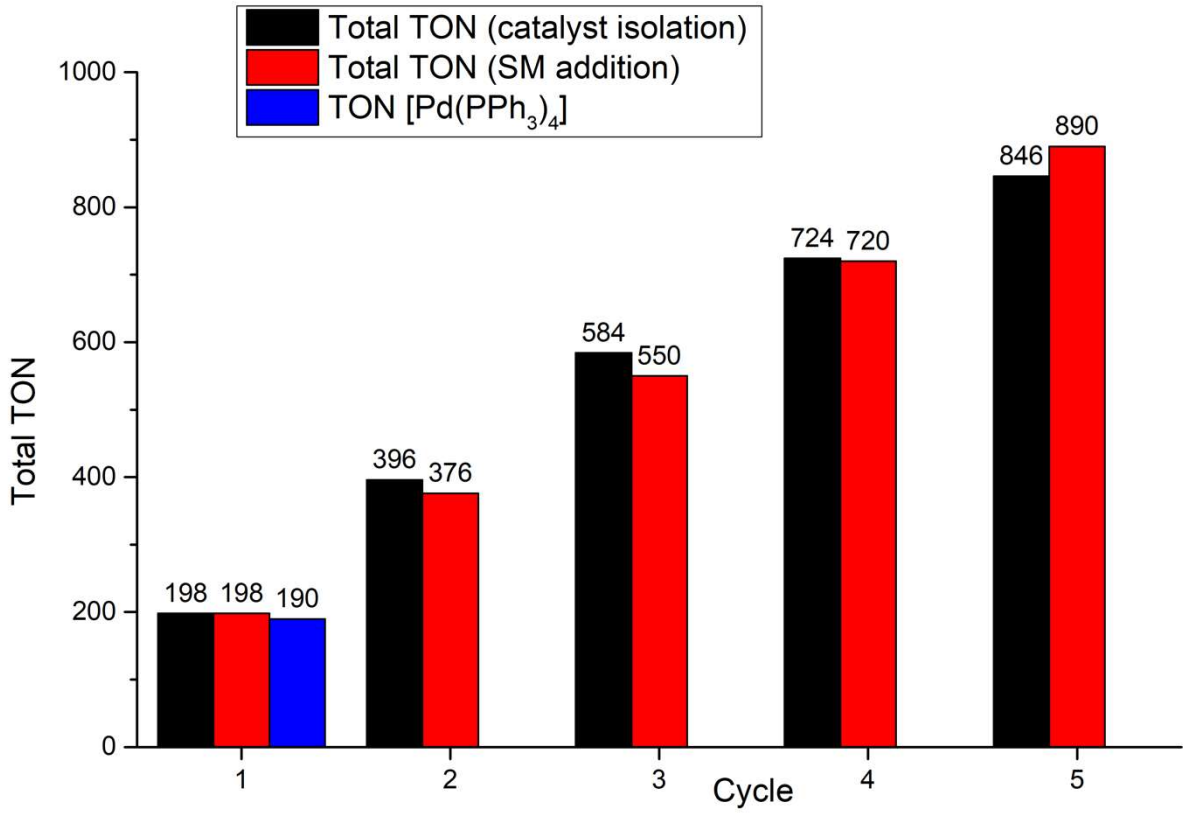

Figure S43. Comparison of TON values for $[Pd(PPh_3)_4]$ and for **Pd@CN-COF** under the recycling conditions of the model reaction **1** + **3** → **4**.

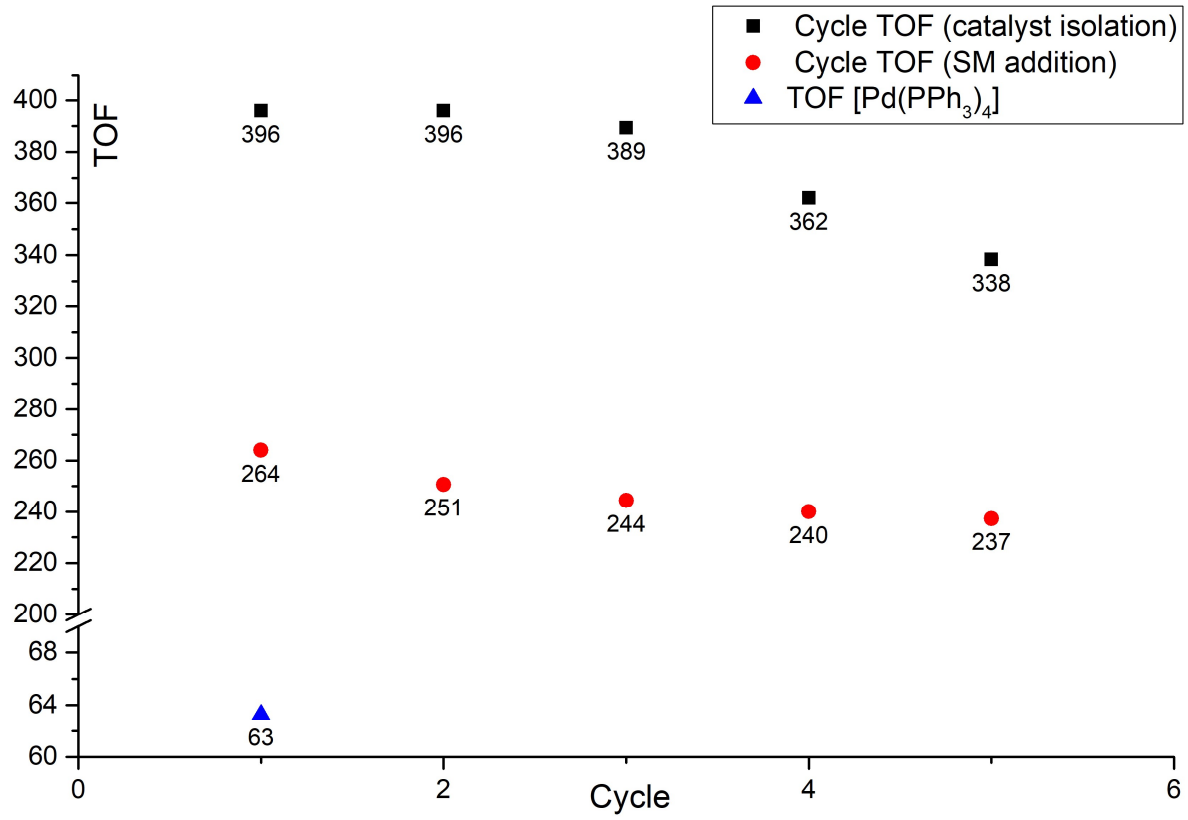

Figure S44. Comparison of TOF values for [Pd(PPh3)4] and **Pd@CN-COF** under the recycling conditions of the model reaction **1** + **3** → **4**.